Title: Reversal of endothelial dysfunction reduces white matter vulnerability in cerebral small vessel disease in rats

Authors: Rikesh M. Rajani[1], Sophie Quick[1], Silvie R. Ruigrok[1], Delyth Graham[2], Sarah E. Harris[3], Benjamin F.J. Verhaaren[4,5], Myriam Fornage[5,6], Sudha Seshadri[5,7], Santosh S. Atanur[8], Anna F. Dominiczak[2], Colin Smith[9], Joanna M. Wardlaw[10], Anna Williams[1*]

Affiliations:

[1]MRC Centre for Regenerative Medicine, and UK Dementia Research Institute at the University of Edinburgh, EH16 4UU, UK

[2]Institute of Cardiovascular and Medical Sciences, University of Glasgow, Glasgow, G12 8QQ, UK

[3]Centre for Cognitive Ageing and Cognitive Epidemiology and MRC Institute of Genetics and Molecular Medicine, University of Edinburgh, Edinburgh, EH4 2LF, UK

[4]Erasmus Medical Centre, 3015 CE Rotterdam, Netherlands

[5]Neurology Working Group of the Cohorts for Heart and Aging Research in Genomic Epidemiology (CHARGE)

[6]Institute of Molecular Medicine, The University of Texas Health Science Center, Houston, TX 77030, USA

[7]Department of Neurology, Boston University School of Medicine, Boston, MA 02118, USA

[8]Centre for Genomic and Experimental Medicine, University of Edinburgh, Edinburgh, EH4 2LF, UK

[9]Academic Neuropathology, Centre for Clinical Brain Sciences, University of Edinburgh, Edinburgh, EH16 4SB, UK

[10]Brain Research Imaging Centre, Centre for Clinical Brain Sciences, and UK Dementia Research Institute at the University of Edinburgh, EH16 4SB, UK

OVERLINE: NEUROPATHOLOGY

*Corresponding author. Email: anna.williams@ed.ac.uk

One Sentence Summary: In cerebral small vessel disease, endothelial dysfunction leads to white matter vulnerability which is reversible in a rat model with endothelial stabilizing drugs.

Abstract: Dementia is a major social and economic problem for our ageing population. One of the commonest causes of dementia in the elderly is cerebral small vessel disease (SVD). Magnetic resonance scans of SVD patients typically show white matter abnormalities, but we do not understand the mechanistic pathological link between blood vessels and white matter myelin damage. Hypertension is suggested as the cause of sporadic SVD, but a recent alternative hypothesis invokes dysfunction of the blood brain barrier as the primary cause. Here, in a rat model of SVD, we show that endothelial cell (EC) dysfunction is the first change in development of the disease. Dysfunctional ECs secrete heat shock protein 90-alpha, which blocks oligodendroglial differentiation, contributing to impaired myelination. Treatment with EC-stabilizing drugs reversed these EC and oligodendroglial pathologies in the rat model. EC and oligodendroglial dysfunction were also observed in humans with early, asymptomatic SVD pathology. We identified a loss-of-function mutation in ATPase11B which caused the EC dysfunction in the rat SVD model, and a single nucleotide polymorphism (SNP) in ATPase11B that was associated with white matter abnormalities in humans with SVD. We show that EC dysfunction is a cause of SVD white matter vulnerability and provide a therapeutic strategy to treat and reverse SVD in the rat model which may also be of relevance to human SVD.

Main text:

Introduction

One of the biggest challenges currently facing society is the increasing number of people with dementia as the population ages. Cerebral small vessel disease (SVD) affects the small perforating arterioles in the brain and is the leading cause of vascular dementia (*1, 2*). SVD also contributes to and worsens the symptoms of Alzheimer's disease (AD) (*2*), and is responsible for up to 45% of dementias. Monogenic forms and some sporadic cases of SVD occur at young ages, which supports SVD as a disease rather than simply being a consequence of aging (*3*). In addition to dementia, SVD causes cognitive impairment, gait and balance problems (*2, 4, 5*), and trebles the risk of stroke (*6*). Its diagnosis relies on clinical presentation of lacunar stroke, or cognitive or gait/balance problems with magnetic resonance imaging (MRI) features such as white matter hyperintensities (WMH) (*7*). These WMH are associated with cognitive decline in SVD (*6*), and pathological diagnosis of SVD relies on characteristic changes such as lipohyalinosis (asymmetric areas of small vessel fibrosis associated with foam cells and leakage of plasma proteins) and myelin loss (*8*) indicating that white matter damage plays an important role in disease pathogenesis.

The risk of sporadic SVD is increased by typical vascular risk factors such as hypertension, diabetes and smoking (*9-11*). Despite one third of people over the age of 80 having some signs of SVD (*12*), there are currently no established SVD therapies (*13*). Most treatments tested in clinical trials so far have focused on blood pressure reduction (*13*), although 30% of SVD patients are normotensive (*14*). Alternatively, some evidence now suggests that blood brain barrier (BBB) changes may cause SVD (*15, 16*). The BBB prevents unwanted cells and solutes in the blood from entering the brain parenchyma and is made of endothelial cells (ECs), pericytes, astrocyte end-feet, and junctions between these cells (*17*). Disruption of the BBB is

found in SVD (*16, 18*), but it is unclear if this causes any observed pathological changes, or is secondary to them.

We sought mechanisms linking vascular changes with white matter pathology by studying the earliest pathological features of SVD in a rat model and human tissue. We show that the first pathological change is EC dysfunction which occurs before the onset of hypertension or clinical signs. We identify both an upstream genetic cause of this EC dysfunction and a secreted downstream effector, impacting surrounding white matter. We also show that drug treatment to stabilize EC dysfunction in a SVD model reverses the endothelial and oligodendroglial pathologies, suggesting a new therapeutic strategy.

Results

To study the early changes in SVD development, we used the stroke-prone spontaneously hypertensive rat [SHRSP; subsequently referred to as disease model (DM)]. This is an inbred rat strain known to be a relevant rodent model of human sporadic SVD (*19, 20*). These DM rats are hypertensive from six weeks, show classical SVD pathology from eight weeks, and suffer strokes from twenty weeks of age (*20-24*). As controls we used the parent strain of the DM rat, Wistar Kyoto rats (WKY), from a colony maintained in parallel. For human tissue, we used brains obtained from people (aged 24-58) who had died suddenly without SVD symptoms but whose brains were found to have early SVD pathology upon post-mortem examination (**table S1**).

BBB changes are found early in a rat SVD model and in humans with pre-symptomatic SVD

Previous work had found BBB changes in DM rats at five weeks of age, predating hypertension (*25*). In deep white matter areas typically affected by SVD pathology, we found that the earliest pathological change seen by immunofluorescence (at four weeks of age) was a decrease in the number of blood vessels expressing claudin-5, the key tight junction protein (TJP) of the BBB, indicative of an altered BBB (*26*) (**Fig. 1A-D, I**). There was also a trend to reduction of the

absolute amount of claudin-5 protein in DM brain at 5 weeks, although this was not statistically significant (**fig. S1**). However, this alteration in claudin-5 expression did not lead to a functional leakage of the BBB to a large dextran tracer in 5-week-old DM rats (**fig. S2**). In the deep white matter of human brains with early stage SVD, we found a similar decrease in blood vessels with colocalized claudin-5 expression (**Fig. 1E-I**). We found no differences in other components of the BBB, including pericytes, astrocytes, astrocyte end-feet, and blood vessel density between DM and control rats, or between the human pre-symptomatic cases and age-relevant controls (**fig. S3**).

OPCs are increased in a rat SVD model and humans with pre-symptomatic SVD

Subsequent to the BBB changes, we found an increase in oligodendrocyte precursor cells (OPCs) in the deep white matter in the DM rat at 5 weeks of age (more $Olig2^+$ Nogo-A^- cells; **Fig. 1J-L**), and also in the human pre-symptomatic cases (**Fig. 1J, M-N**). This increase was due to both a block in OPC differentiation to mature oligodendrocytes (fewer mature $Olig2^+$ Nogo-A^+ oligodendrocytes; **Fig. 1O**), and an increase in OPC proliferation (**Fig. 1P, fig. S4**). We also found an increase in the number of macrophages/microglia at five weeks of age in the DM rats (**fig. S5A-B, E**) and in the human cases (**fig. S5C-E**), suggestive of a secondary immune response.

Early changes occur without hypertension or leakage through the BBB

The order of these changes in the DM rat suggests that an early change in the ECs contributes to the later white matter changes and occurs well before the rats become hypertensive. However, the lack of a functional leak in DM rats in vivo at this early time point suggests that early white matter pathology does not result from substances in the blood leaking through an impaired BBB. To confirm this, we cultured brain slices from neonatal DM rats ex vivo for five weeks, in the absence of blood flow and blood pressure. We observed the same changes as at 5 weeks in vivo: a reduction in claudin-5 protein expression (**Fig. 2A-B**), an increase in OPC number (more

Olig2^{+} Nogo-A^{-} cells; **Fig. 2C-E**), and a reduction in mature oligodendrocytes (fewer Olig2^{+} Nogo-A^{+} oligodendrocytes; **Fig. 2F**). As these data confirm that neither BBB leakage nor hypertension caused the early myelin pathology in this model, we next considered endothelial dysfunction as a mechanism for the pathology.

DM rats and human SVD brains have dysfunctional ECs

Endothelial dysfunction is commonly defined as a reduction in the bioavailability of nitric oxide (NO) in an endothelial cell (EC) (*27*). This may be due to either a reduction in NO production by endothelial nitric oxide synthase (eNOS), or an increase in NO sequestration by superoxide. At 3 weeks of age, before tight junction changes are seen in blood vessels, brains of DM rats already showed reduced eNOS compared to controls (**Fig. 2G-H**). Dysfunctional ECs also have a high proliferation rate (*28, 29*), and we found more proliferating ECs in both 3-week-old DM rat tissue and diseased human brains compared to controls (**Fig. 2I-M**). To determine whether this dysfunction was cell autonomous, we isolated and cultured brain microvascular endothelial cells (BMECs) from neonatal DM and control rats and found that DM cells produced less NO (**Fig. 2N**). DM BMECS also showed reduced tight junction integrity. Control BMECs expressed zonula occludens 1 (ZO-1) (a marker of tight junctions) and claudin-5 (a marker of mature tight junctions) in their cell membranes. In comparison, DM BMECs expressed ZO-1 normally but showed reduced claudin-5 localization in their membranes (**Fig. 2O-R**).

Dysfunctional ECs reduce OPC maturation and increase OPC proliferation

To investigate whether dysfunctional ECs secrete factors that cause the white matter changes in the DM rat, we collected conditioned media from DM BMECs and added it to in vitro cultures of wild-type OPCs. Treatment with DM BMEC conditioned media led to a reduction in maturation of wild-type OPCs (more immature NG2^{+} OPCs, fewer mature MBP^{+} oligodendrocytes; **Fig. 3A-D**) and more proliferation (**Fig. 3E-G**) compared to wild-type OPCs grown in control BMEC conditioned media. Furthermore, ex vivo slice cultures grown in DM

BMEC conditioned media contained more OPCs than slices grown in control BMEC conditioned media (**Fig. 3H-J**). Therefore, secreted factors from DM BMECs affect oligodendroglia biology, blocking OPC maturation and increasing their proliferation. This correlates with the findings seen in tissue sections from young DM rat brains, and pre-symptomatic diseased human brains.

HSP90α secreted by ECs mediates the reduction in OPC maturation

To identify these soluble factors secreted from DM BMECs, we used a forward phase antibody microarray with >1300 antibodies against select proteins. One protein expressed more in DM compared to control BMEC conditioned media was heat shock protein 90 alpha (HSP90α) (**fig. S6**), a chaperone protein highly expressed in all brain cell types. We confirmed increased protein in DM BMEC conditioned media by western blot (**Fig. 3K-L**) and saw a trend to an increase on enzyme-linked immunosorbent assay (ELISA)(P=0.05) (**Fig. 3M**). Treatment of OPCs with recombinant HSP90α (rHSP90α) decreased OPC maturation (more immature $NG2^+$ OPCs, fewer mature MBP^+ oligodendrocytes; **Fig. 3N-Q**), mirroring the effect seen with DM BMEC conditioned media, but had no effect on OPC proliferation compared to controls (**fig. S7A-C**). A blocking antibody specific to HSP90α abrogated the DM BMEC conditioned media-induced maturation defects (**Fig. 3R-V**), but again OPC proliferation was unchanged (**fig. S7D-G**). These data show that HSP90α secreted by DM BMECs causes the block in maturation of OPCs, but is not responsible for the proliferation effect. Furthermore, we found more of the cleaved, secreted form of HSP90α (*30*) in DM rat brains (**Fig. 3W-X**) and in some diseased human brains (**Fig. 3W,Y**), suggesting that a similar mechanism downstream of endothelial dysfunction also occurs in human SVD.

Drugs which ameliorate endothelial dysfunction reverse OPC changes in vivo

We next investigated whether reducing endothelial dysfunction improves white matter pathology in vivo. We treated DM rats with drugs reported to reduce endothelial dysfunction: simvastatin, a cholesterol lowering drug; perindopril, an angiotensin-converting enzyme inhibitor (ACEI); or

cilostazol, a phosphodiesterase inhibitor (*31-34*). We dosed animals from five weeks old, a time point at which both endothelial and OPC pathologies are present, to adulthood at twelve weeks (**Fig. 4A**). These animals were compared to untreated WKY rats, untreated DM rats, and animals treated with a combination drug [hydralazine and hydrochlorothiazide (H+H)] that lowers blood pressure but does not alter endothelial dysfunction, as a control for the blood pressure reduction expected with perindopril (**Fig. 4B; table S2**). Blood pressures were monitored weekly, and increased in all rats over time (as expected as they mature to adulthood) (*35*) but clustered into two groups: one with high blood pressure (untreated DM rats and rats treated with simvastatin or cilostazol) and the other with normal blood pressure (DM rats treated with the anti-hypertensives perindopril or H+H and untreated WKY rats) (**Fig. 4C**).

At twelve weeks, we examined the brains for signs of endothelial dysfunction and white matter changes. Simvastatin and perindopril significantly reduced EC proliferation ($P<0.001$ for both) (**Fig. 4D-E, L**) and significantly increased mature TJs in the DM rats ($P<0.05$ for both) (**Fig. 4F-G, M**), confirming that these drugs improve endothelial dysfunction. Cilostazol showed trend effects only in the same direction. Simvastatin, perindopril and cilostazol reversed the increase in OPCs seen in untreated DM rats ($P<0.001$, $P<0.001$ and $P<0.01$ respectively) (**Fig. 4H-I, N**). In the case of simvastatin and perindopril, this is by both reducing the OPC differentiation block ($P<0.001$ for both) (**Fig. 4O**) and reducing OPC proliferation ($P<0.01$ for simvastatin, $P<0.05$ for perindopril) **(Fig. 4J-K, P)**. Cilostazol only showed a significant increase in mature oligodendrocytes ($P<0.001$) (**Fig. 4P**). Furthermore, blinded ranking of the quality of myelin in the deep white matter areas showed a pattern of less myelin rarefaction in DM rats treated with drugs reducing EC dysfunction, with a significant reduction for simvastatin ($P<0.01$) (**Fig. 4Q).** These data demonstrate that improving endothelial dysfunction reverses the oligodendroglial changes in DM rats in vivo, further demonstrating that these are secondary to endothelial dysfunction. These drugs act via different pharmacological pathways, suggesting that endothelial

dysfunction reversal itself is the key therapeutic mechanism. This effect is also independent of blood pressure, as normotensive DM rats treated with H+H showed little improvement, and hypertensive DM rats treated with simvastatin and cilostazol showed significant improvements in pathology.

DM rats have a homozygous deletion in *Atp11b*

We next sought to identify the cause of the endothelial dysfunction in our inbred DM rats. We reanalyzed published genomic array sequencing data of the DM rat (SHRSP), the spontaneously hypertensive rat (SHR, which is its closest related strain and develops hypertension but does not show signs of SVD or stroke), and the control strain [the Wistar Kyoto rat (WKY)] (*36*). As a first pass analysis, we examined the lists of frameshift mutations and single nucleotide variants that introduce stop codons, as these would be expected to lead to a truncated protein. We selected genes with homozygous mutations occurring in SHRSP but not in SHR, with the assumption that genes mutated in both contribute to the hypertensive phenotype common to both strains, not the SVD phenotype unique to SHRSP. We then filtered this resulting list of 32 genes further (**Fig. 5A**) using ENSEMBL's Variant Effect Predictor tool (*37*) to select mutations resulting in a truncated protein, the Allen Brain Atlas (*38*) to select only those genes expressed in the brain, and the Barres Brain RNA-Seq database (*39*) to select genes expressed in brain ECs, as our earlier results demonstrated that the mutation which causes endothelial dysfunction is cell autonomous. This reduced the list to six genes. Using Sanger sequencing, only one gene was confirmed to have the predicted mutation present in an exon (hence coding and leading to a truncated protein): ATPase, Class VI, type 11B (*Atp11b*) (**Fig. 5B**). By western blot we showed that this mutation causes a total loss of ATP11B protein rather than the predicted truncated protein (**Fig. 5C**).

Knockdown of *Atp11b* in ECs phenocopies DM BMECs

To investigate whether deletion of *Atp11b* causes the endothelial dysfunction observed in our DM rats, we knocked down the gene using siRNA in an endothelial cell line (bEND.3), achieving a 61% ± 20% knockdown (KD) of protein (**Fig. 5D-E**). *Atp11b*-KD bEND.3 cells showed signs of endothelial dysfunction, with a higher proliferation rate (**Fig. 5F-H**) and formation of less mature TJs (**Fig. 5I-L)** than cells treated with non-targeting siRNA. Treatment of OPCs with conditioned media collected from *Atp11b*-KD bEND.3 cells caused a block in OPC maturation (more immature $NG2^+$ OPCs, and fewer mature MBP^+ oligodendrocytes; **Fig. 5M-P**) and increased proliferation **(Fig. 5Q-S**). Similarly, conditioned media from human endothelial cells treated with siRNAs to knockdown *ATP11B* led to a block in rat OPC maturation (more $NG2^+$ OPCs, fewer mature MBP^+ oligodendrocytes, proportional to amount of knockdown) (**fig. S8**). [Of note, the commercial human cerebral endothelial cell lines HBEC5i and hCMEC/d3 did not express endothelial markers and therefore were not used (**fig. S9**)]. Furthermore, *Atp11b*-KD bEND.3 cells secreted more HSP90α compared to those treated with non-targeting siRNA (**Fig. 5T-U**), linking the upstream and downstream pathways, and suggesting a similar mechanism of action to DM BMECs.

A SNP in *ATP11B* is associated with WMH in humans

To determine if *ATP11B* is relevant to SVD in humans, we obtained summary data from a previous study which investigated the genome-wide association of single nucleotide polymorphisms (SNPs) with WMH burden assessed by MRI (*40*). This study included 17,936 individuals of European descent from 29 population-based cohorts, as part of the Cohorts for Heart and Aging Research in Genomic Epidemiology (CHARGE) consortium (http://www.chargeconsortium.com). SNPs were imputed from the 1000 Genomes reference and WMH burden was quantified on MRI by either automated segmentation or a visual rating scale. We looked at 304 SNPs within *ATP11B* and found seven SNPs which were significantly associated with WMH ($P<0.05$; **fig. S10**). After correcting for multiple testing, using spectral

decomposition to determine the number of independent SNPs tested using the 1000 Genomes reference as a measure of linkage disequilibrium (*41*), we found one intronic SNP which was associated with WMH burden: rs148771930 (P=0.00025).

We used the Genotype-Tissue Expression Portal (GTEx) (http://www.gtexportal.org) to try to identify expression quantitative trait loci (eQTL) associated with this SNP but none was identified. We also interrogated Regulome DB database46 (http://www.regulomedb.org/) to identify regulatory DNA elements in non-coding and intergenic regions of the genome in normal cell lines and tissues. Minimal binding evidence was identified (Regulome DB score = 6), but this included a position weight matrix motif and evidence of histone modifications, suggesting that the SNP may be involved in gene regulation. Although the functional effect of this SNP is not clear, its association with WMH in this dataset suggests that *ATP11B* may also be important in the pathogenesis of the human disease.

A summary of our model is shown in **fig. S11**.

Discussion

Here, we demonstrated that endothelial dysfunction is an early precipitant of disease development in a rat model of SVD and a sample of humans with sporadic SVD. We identified a deletion in *Atp11b* and loss of ATP11B protein as causing endothelial dysfunction, with abnormalities of the BBB TJs, increased EC proliferation, and reduction in eNOS and NO. This dysfunction led to secretion of factors, including HSP90α, which blocked the maturation of OPCs into myelinating oligodendrocytes, consistent with the impairment of myelination and inherent vulnerability of white matter to damage seen in adult humans with SVD (*42*). We also demonstrated therapeutic reversal of endothelial dysfunction and associated reduction in white matter vulnerability. The early reduction of the BBB TJ markers but lack of tracer leakage (along with the brain slice culture experiments) showed that leakage of substances through the BBB is

not important for initial SVD pathology in our model. However, it is highly likely that BBB leakage is important for later worsening of pathology, as fibrinogen is found around the blood vessels both in late human disease and in the rat SVD model.

There are many possible upstream causes of endothelial dysfunction in SVD, both environmental and genetic. The common environmental risk factors for SVD, such as hypertension, smoking and diabetes, can induce endothelial dysfunction (*43-45*), reconciling the epidemiological associations of SVD. SVD patients have elevated plasma concentrations of soluble biomarkers of endothelial dysfunction, such as ICAM-1 (*46*), and impaired vasodilation in response to vasoactive challenges (*47*). Animal models of monogenic forms of SVD [such as cerebral autosomal dominant arteriopathy with subcortical infarcts and leukoencephalopathy (CADASIL) and *COL4A1* mutations] show reduced vascular reactivity, a sign of endothelial dysfunction (*48, 49*). Genetic polymorphisms in the gene coding for eNOS, which reduce eNOS activity, are associated with SVD (*50, 51*).

We found a mutation in *Atp11b* as an upstream cause of endothelial dysfunction in the DM rat. We confirmed that a knock down of *Atp11b* or *ATP11B* in wild-type rodent and human ECs induced a similar dysfunctional EC phenotype, including an increase in secretion of HSP90α and the secondary effects on OPCs. We also showed that this gene may play a role in human SVD, as a SNP in *ATP11B* was associated with WMH burden. ATP11B is a member of the phospholipid flippase family of proteins, responsible for moving phospholipids from the outer/luminal leaflet of the plasma or organelle membrane to the inner/cytoplasmic leaflet (*52*). ATP11B specifically is involved in vesicular transport from the trans Golgi network to the plasma membrane (*53*). As the localization of the enzyme eNOS, which shuttles between the Golgi and the plasma membrane, is critical for its ability to produce sufficient NO (*54*), we hypothesize but have not yet shown that loss of ATP11B may cause endothelial dysfunction by altering the location and hence the activity of eNOS.

Downstream of endothelial dysfunction, we showed that HSP90α is an important factor secreted from dysfunctional ECs which mediates the oligodendroglial maturation defect. The mechanism of action of this OPC maturation block is unknown, but HSP90α, acting through the receptor low density lipoprotein receptor-related protein 1 (LRP-1), can regulate the Akt pathway (*55*), which is key in OPC maturation (*56, 57*). We also saw increased secretion of HSP90α in brains from humans with sporadic pre-symptomatic SVD. Therefore, this factor may be downstream of a common pathway of endothelial dysfunction from different causes. Although signaling from OPCs to ECs has been studied previously (*58, 59*), there is less reported on the effects of ECs on OPCs (*60-62*), in spite of the increasing evidence that SVD patients have dysfunctional ECs and the link between early life predictors of white matter vulnerability and later SVD (*42, 63, 64*).

There is MRI evidence of WMH improving in humans with SVD (*64*). We showed that it was possible to reverse endothelial dysfunction and white matter abnormalities with EC-stabilizing drugs in the early disease state in the rat SVD model. These drugs include statins, which have previously been shown to reduce stroke occurrence in SVD patients, but only in patients with elevated cholesterol (*65*). Endothelial dysfunction and OPC changes were also reversed with ACEIs, but not with anti-hypertensives that do not stabilize ECs. Anti-hypertensives have been extensively tested in clinical trials in human SVD with mixed results (*13*), perhaps secondary to use of different classes of anti-hypertensive drugs with different effects on endothelial dysfunction. In fact, trials that exclusively use ACEIs have shown more positive effects on preventing WMH progression in SVD (*66*). Cilostazol acts on ECs through a third mechanism and is currently in early stage clinical trials for SVD (Clinical trial: ISRCTN12580546).

Our study has raised as yet unanswered questions. We do not yet know whether this pathology is reversible later in the disease, when leak of blood components through the BBB is also present and whether these treatments may also have an impact on the clinical behavior of the DM rats. Although this rat model is well-recognized as an appropriate model of human SVD, it would be

interesting to determine whether a similar mechanism of disease is present in other models including single gene mutation models mirroring human genetic forms of SVD. To determine whether treatment of humans with drugs which stabilize ECs is associated with a better outcome in SVD, it would also be interesting to re-assess stroke clinical trial data comparing EC-stabilizing treatment groups with other non-EC stabilizing antihypertensives.

In this study, we show a primary, non-ischemic mechanism of endothelial dysfunction in SVD and how this leads to the white matter pathology. We identified a SNP in a gene expressed in endothelial cells in humans that may contribute to vulnerability to SVD. We emphasize that endothelial cell function consists of more than just controlling blood flow, and that the interactions of endothelial cells and other brain cells – in particular, oligodendroglia – are central to this disease process. We propose that endothelial dysfunction plays a major, causative role in SVD, and that reversal of endothelial dysfunction is therapeutic target for effective treatment for this common, disabling, multifactorial disease, with potential for high societal health impact.

Materials and Methods

Study design

The overall goal of this study was to determine the mechanism of pathology in cerebral SVD, using early pre-symptomatic human tissue and a rat model of the disease. The use of human tissue for this study was approved by the Medical Research Council Edinburgh Brain and Tissue Bank. This bank has ethical approval to collect tissue for research after informed consent from the next of kin. All animal experiments were carried out in line with UK Home Office guidelines, under project licences 60/4268 (D.G.), 70/9021 (D.G) and 60/4524 (A.W.). Treatment groups were randomly assigned, data were analyzed by blinded observers, and biological replicate numbers are stated with each result along with the statistical test used. Stroke-prone spontaneously hypertensive rats (SHRSP) and matched control strain, Wistar Kyoto rats (WKY),

were housed at the University of Glasgow. Animals were fed standard chow and housed in line with Home Office guidelines. Breeding SHRSP pairs regularly had their blood pressure tested to ensure maintenance of the colony's phenotype. Male animals were exclusively used for both WKY controls and SHRSPs as SHRSP males display a more severe phenotype. Sprague Dawley rats housed at the University of Edinburgh were used for wild-type OPCs and slice cultures.

Drug study.

Animals used in the drug study were individually housed and fed the drugs mixed in with highly palatable baby food daily from the age of 5 weeks, after pathology first appears, to the age of 12 weeks. Animals were treated in 5 batches, with each batch containing one animal randomly assigned to each treatment group. Analysis suggested a minimum of 5 animals per treatment group to detect an effect size of 35% with 80% power (*67*). One animal which died before the age of 12 weeks without stroke pathology was not included in the final analysis. Drugs were administered at doses based on previously published data demonstrating their efficacy at either lowering blood pressure or improving endothelial dysfunction when administered orally in rats: simvastatin (Sigma): 2 mg/kg/day (*32, 33*); perindopril (Sigma): 2 mg/kg/day (*68*); cilostazol (Sigma): 60 mg/kg/day (*69*); hydrochlorothiazide and hydralazine (Sigma): 16 mg/kg/day of each (*70*) (**table S2**). Blood pressure was measured before treatment, and weekly after treatment started, by tail-cuff plethysmography. Myelin rarefaction was ranked blind to group from Luxol fast blue/Cresyl violet stained sections.

Human tissue

Human tissue was provided as paraffin embedded blocks by the MRC Edinburgh Sudden Death Brain Bank. All blocks were from the deep white matter of patients who died suddenly without clinical signs of SVD. Five blocks were chosen from people who had histopathological signs of

SVD upon post-mortem examination by a Neuropathologist (CS) and five matched controls (age: control: 46 ± 16 (mean ± standard deviation), SVD: 49 ± 14; post-mortem interval: control: 60 ± 20 hours, SVD: 58 ± 25 hours; percentage male: control: 100%, SVD 60%) were chosen from people with no post-mortem signs of SVD. Full details of the human tissue, including histopathological signs of SVD, are provided in **table S1**. Unique identifying numbers (MRC database numbers): SD015/08 (BBN2434), SD021/08 (BBN2440), SD034/08 (BBN2453), SD014/09 (BBN2473), SD010/10 (BBN2507), SD019/08 (BBN2438), SD020/08 (BBN2439), SD022/08 (BBN2481) SD023/08 (BBN2442), SD031/08 (BBN2450).

Statistical analysis

Graphs were produced and statistics calculated using GraphPad Prism software. Data are presented as mean ± standard error of the mean (SEM), comparing at least three biological repeats each time. Numbers and type of biological repeats are stated in each graphical figure legend. For in vitro studies, an experiment is defined as using cells or slices prepared at different times from different animals or passages. For comparisons between two groups, significance was determined using a two-tailed Student's t-test, either paired (for in vitro experiments where the control and experimental conditions were run in parallel for each biological repeat) or unpaired. For experiments with multiple comparisons, a one-way or two-way ANOVA was used as appropriate (repeated measures for in vitro experiments), with post-hoc Bonferroni or Tukey's tests to determine significance between groups. Statistical significance was defined as $P<0.05$.

Supplementary Materials:

Materials and Methods

Fig. S1. Lower claudin-5 protein in brains of DM rats.

References:

1. M. M. Esiri, G. K. Wilcock, J. H. Morris, Neuropathological assessment of the lesions of significance in vascular dementia. *J Neurol Neurosurg Psychiatry* **63**, 749-753 (1997).
2. A. Smallwood, A. Oulhaj, C. Joachim, S. Christie, C. Sloan, A. D. Smith, M. Esiri, Cerebral subcortical small vessel disease and its relation to cognition in elderly subjects: a pathological study in the Oxford Project to Investigate Memory and Ageing (OPTIMA) cohort. *Neuropathol Appl Neurobiol* **38**, 337-343 (2012).
3. C. Haffner, R. Malik, M. Dichgans, Genetic factors in cerebral small vessel disease and their impact on stroke and dementia. *J Cereb Blood Flow Metab* **36**, 158-171 (2016).
4. K. F. de Laat, A. M. Tuladhar, A. G. van Norden, D. G. Norris, M. P. Zwiers, F. E. de Leeuw, Loss of white matter integrity is associated with gait disorders in cerebral small vessel disease. *Brain* **134**, 73-83 (2011).
5. N. D. Prins, E. J. van Dijk, T. den Heijer, S. E. Vermeer, J. Jolles, P. J. Koudstaal, A. Hofman, M. M. Breteler, Cerebral small-vessel disease and decline in information processing speed, executive function and memory. *Brain* **128**, 2034-2041 (2005).
6. S. Debette, H. S. Markus, The clinical importance of white matter hyperintensities on brain magnetic resonance imaging: systematic review and meta-analysis. *BMJ* **341**, c3666 (2010).
7. J. M. Wardlaw, E. E. Smith, G. J. Biessels, C. Cordonnier, F. Fazekas, R. Frayne, R. I. Lindley, J. T. O'Brien, F. Barkhof, O. R. Benavente, S. E. Black, C. Brayne, M. Breteler, H. Chabriat, C. Decarli, F. E. de Leeuw, F. Doubal, M. Duering, N. C. Fox, S. Greenberg, V. Hachinski, I. Kilimann, V. Mok, R. Oostenbrugge, L. Pantoni, O. Speck, B. C. Stephan, S. Teipel, A. Viswanathan, D. Werring, C. Chen, C. Smith, M. van Buchem, B. Norrving, P. B. Gorelick, M. Dichgans, S. T. f. R. V. c. o. nEuroimaging, Neuroimaging standards for research into small vessel disease and its contribution to ageing and neurodegeneration. *Lancet Neurol* **12**, 822-838 (2013).
8. E. L. Bailey, C. Smith, C. L. Sudlow, J. M. Wardlaw, Pathology of lacunar ischemic stroke in humans--a systematic review. *Brain Pathol* **22**, 583-591 (2012).
9. A. G. Thrift, J. J. McNeil, A. Forbes, G. A. Donnan, Three important subgroups of hypertensive persons at greater risk of intracerebral hemorrhage. Melbourne Risk Factor Study Group. *Hypertension* **31**, 1223-1229 (1998).
10. W. S. Ryu, S. H. Woo, D. Schellingerhout, M. K. Chung, C. K. Kim, M. U. Jang, K. J. Park, K. S. Hong, S. W. Jeong, J. Y. Na, K. H. Cho, J. T. Kim, B. J. Kim, M. K. Han, J. Lee, J. K. Cha, D. H. Kim, S. J. Lee, Y. Ko, Y. J. Cho, B. C. Lee, K. H. Yu, M. S. Oh, J. M. Park, K. Kang, K. B. Lee, T. H. Park, J. Lee, H. K. Choi, K. Lee, H. J. Bae, D. E. Kim, Grading and interpretation of white matter hyperintensities using statistical maps. *Stroke* **45**, 3567-3575 (2014).
11. E. J. van Dijk, N. D. Prins, H. A. Vrooman, A. Hofman, P. J. Koudstaal, M. M. Breteler, Progression of cerebral small vessel disease in relation to risk factors and cognitive consequences: Rotterdam Scan study. *Stroke* **39**, 2712-2719 (2008).
12. S. E. Vermeer, W. T. Longstreth, Jr., P. J. Koudstaal, Silent brain infarcts: a systematic review. *Lancet Neurol* **6**, 611-619 (2007).
13. P. M. Bath, J. M. Wardlaw, Pharmacological treatment and prevention of cerebral small vessel disease: a review of potential interventions. *Int J Stroke* **10**, 469-478 (2015).
14. G. A. Lammie, F. Brannan, J. Slattery, C. Warlow, Nonhypertensive cerebral small-vessel disease. An autopsy study. *Stroke* **28**, 2222-2229 (1997).
15. J. M. Wardlaw, P. A. Sandercock, M. S. Dennis, J. Starr, Is breakdown of the blood-brain barrier responsible for lacunar stroke, leukoaraiosis, and dementia? *Stroke* **34**, 806-812 (2003).
16. A. J. Farrall, J. M. Wardlaw, Blood-brain barrier: ageing and microvascular disease--systematic review and meta-analysis. *Neurobiol Aging* **30**, 337-352 (2009).
17. N. J. Abbott, L. Ronnback, E. Hansson, Astrocyte-endothelial interactions at the blood-brain barrier. *Nat Rev Neurosci* **7**, 41-53 (2006).
18. J. M. Wardlaw, S. J. Makin, M. C. Valdés Hernández, P. A. Armitage, A. K. Heye, F. M. Chappell, S. Muñoz-Maniega, E. Sakka, K. Shuler, M. S. Dennis, M. J. Thrippleton, Blood-brain

barrier failure as a core mechanism in cerebral small vessel disease and dementia: evidence from a cohort study. *Alzheimer's & Dementia* **13**, 634-643 (2017).
19. A. H. Hainsworth, H. S. Markus, Do in vivo experimental models reflect human cerebral small vessel disease? A systematic review. *J Cereb Blood Flow Metab* **28**, 1877-1891 (2008).
20. E. L. Bailey, C. Smith, C. L. Sudlow, J. M. Wardlaw, Is the spontaneously hypertensive stroke prone rat a pertinent model of sub cortical ischemic stroke? A systematic review. *Int J Stroke* **6**, 434-444 (2011).
21. Y. Yamori, R. Horie, Developmental course of hypertension and regional cerebral blood flow in stroke-prone spontaneously hypertensive rats. *Stroke* **8**, 456-461 (1977).
22. J. X. Lin, H. Tomimoto, I. Akiguchi, H. Wakita, H. Shibasaki, R. Horie, White matter lesions and alteration of vascular cell composition in the brain of spontaneously hypertensive rats. *Neuroreport* **12**, 1835-1839 (2001).
23. Y. Yamori, R. Horie, H. Handa, M. Sato, M. Fukase, Pathogenetic similarity of strokes in stroke-prone spontaneously hypertensive rats and humans. *Stroke* **7**, 46-53 (1976).
24. J. A. Gratton, A. Sauter, M. Rudin, K. R. Lees, J. McColl, J. L. Reid, A. F. Dominiczak, I. M. Macrae, Susceptibility to cerebral infarction in the stroke-prone spontaneously hypertensive rat is inherited as a dominant trait. *Stroke* **29**, 690-694 (1998).
25. E. L. Bailey, J. M. Wardlaw, D. Graham, A. F. Dominiczak, C. L. Sudlow, C. Smith, Cerebral small vessel endothelial structural changes predate hypertension in stroke-prone spontaneously hypertensive rats: a blinded, controlled immunohistochemical study of 5- to 21-week-old rats. *Neuropathol Appl Neurobiol* **37**, 711-726 (2011).
26. T. Nitta, M. Hata, S. Gotoh, Y. Seo, H. Sasaki, N. Hashimoto, M. Furuse, S. Tsukita, Size-selective loosening of the blood-brain barrier in claudin-5-deficient mice. *J Cell Biol* **161**, 653-660 (2003).
27. D. G. Harrison, Cellular and molecular mechanisms of endothelial cell dysfunction. *J Clin Invest* **100**, 2153-2157 (1997).
28. M. Drab, P. Verkade, M. Elger, M. Kasper, M. Lohn, B. Lauterbach, J. Menne, C. Lindschau, F. Mende, F. C. Luft, A. Schedl, H. Haller, T. V. Kurzchalia, Loss of caveolae, vascular dysfunction, and pulmonary defects in caveolin-1 gene-disrupted mice. *Science* **293**, 2449-2452 (2001).
29. G. Rajashekhar, A. Willuweit, C. E. Patterson, P. Sun, A. Hilbig, G. Breier, A. Helisch, M. Clauss, Continuous endothelial cell activation increases angiogenesis: evidence for the direct role of endothelium linking angiogenesis and inflammation. *J Vasc Res* **43**, 193-204 (2006).
30. X. Wang, X. Song, W. Zhuo, Y. Fu, H. Shi, Y. Liang, M. Tong, G. Chang, Y. Luo, The regulatory mechanism of Hsp90alpha secretion and its function in tumor malignancy. *Proc Natl Acad Sci U S A* **106**, 21288-21293 (2009).
31. T. F. Luscher, Endothelial dysfunction: the role and impact of the renin-angiotensin system. *Heart* **84 Suppl 1**, i20-22:discussion i50 (2000).
32. M. Alvarez de Sotomayor, C. Perez-Guerrero, M. D. Herrera, E. Marhuenda, Effects of chronic treatment with simvastatin on endothelial dysfunction in spontaneously hypertensive rats. *J Hypertens* **17**, 769-776 (1999).
33. J. Carneado, M. Alvarez de Sotomayor, C. Perez-Guerrero, L. Jimenez, M. D. Herrera, E. Pamies, M. D. Martin-Sanz, P. Stiefel, M. Miranda, L. Bravo, E. Marhuenda, Simvastatin improves endothelial function in spontaneously hypertensive rats through a superoxide dismutase mediated antioxidant effect. *J Hypertens* **20**, 429-437 (2002).
34. A. Hashimoto, G. Miyakoda, Y. Hirose, T. Mori, Activation of endothelial nitric oxide synthase by cilostazol via a cAMP/protein kinase A- and phosphatidylinositol 3-kinase/Akt-dependent mechanism. *Atherosclerosis* **189**, 350-357 (2006).
35. H. H. Koh-Tan, M. Dashti, T. Wang, W. Beattie, J. McClure, B. Young, A. F. Dominiczak, M. W. McBride, D. Graham, Dissecting the genetic components of a quantitative trait locus for blood pressure and renal pathology on rat chromosome 3. *J Hypertens* **35**, 319-329 (2017).
36. S. S. Atanur, A. G. Diaz, K. Maratou, A. Sarkis, M. Rotival, L. Game, M. R. Tschannen, P. J. Kaisaki, G. W. Otto, M. C. Ma, T. M. Keane, O. Hummel, K. Saar, W. Chen, V. Guryev, K. Gopalakrishnan, M. R. Garrett, B. Joe, L. Citterio, G. Bianchi, M. McBride, A. Dominiczak, D. J. Adams, T. Serikawa, P. Flicek, E. Cuppen, N. Hubner, E. Petretto, D. Gauguier, A. Kwitek, H.

Jacob, T. J. Aitman, Genome sequencing reveals loci under artificial selection that underlie disease phenotypes in the laboratory rat. *Cell* **154**, 691-703 (2013).

37. F. Cunningham, M. R. Amode, D. Barrell, K. Beal, K. Billis, S. Brent, D. Carvalho-Silva, P. Clapham, G. Coates, S. Fitzgerald, L. Gil, C. G. Giron, L. Gordon, T. Hourlier, S. E. Hunt, S. H. Janacek, N. Johnson, T. Juettemann, A. K. Kahari, S. Keenan, F. J. Martin, T. Maurel, W. McLaren, D. N. Murphy, R. Nag, B. Overduin, A. Parker, M. Patricio, E. Perry, M. Pignatelli, H. S. Riat, D. Sheppard, K. Taylor, A. Thormann, A. Vullo, S. P. Wilder, A. Zadissa, B. L. Aken, E. Birney, J. Harrow, R. Kinsella, M. Muffato, M. Ruffier, S. M. Searle, G. Spudich, S. J. Trevanion, A. Yates, D. R. Zerbino, P. Flicek, Ensembl 2015. *Nucleic Acids Res* **43**, D662-669 (2015).
38. E. S. Lein, M. J. Hawrylycz, N. Ao, M. Ayres, A. Bensinger, A. Bernard, A. F. Boe, M. S. Boguski, K. S. Brockway, E. J. Byrnes, L. Chen, L. Chen, T. M. Chen, M. C. Chin, J. Chong, B. E. Crook, A. Czaplinska, C. N. Dang, S. Datta, N. R. Dee, A. L. Desaki, T. Desta, E. Diep, T. A. Dolbeare, M. J. Donelan, H. W. Dong, J. G. Dougherty, B. J. Duncan, A. J. Ebbert, G. Eichele, L. K. Estin, C. Faber, B. A. Facer, R. Fields, S. R. Fischer, T. P. Fliss, C. Frensley, S. N. Gates, K. J. Glattfelder, K. R. Halverson, M. R. Hart, J. G. Hohmann, M. P. Howell, D. P. Jeung, R. A. Johnson, P. T. Karr, R. Kawal, J. M. Kidney, R. H. Knapik, C. L. Kuan, J. H. Lake, A. R. Laramee, K. D. Larsen, C. Lau, T. A. Lemon, A. J. Liang, Y. Liu, L. T. Luong, J. Michaels, J. J. Morgan, R. J. Morgan, M. T. Mortrud, N. F. Mosqueda, L. L. Ng, R. Ng, G. J. Orta, C. C. Overly, T. H. Pak, S. E. Parry, S. D. Pathak, O. C. Pearson, R. B. Puchalski, Z. L. Riley, H. R. Rockett, S. A. Rowland, J. J. Royall, M. J. Ruiz, N. R. Sarno, K. Schaffnit, N. V. Shapovalova, T. Sivisay, C. R. Slaughterbeck, S. C. Smith, K. A. Smith, B. I. Smith, A. J. Sodt, N. N. Stewart, K. R. Stumpf, S. M. Sunkin, M. Sutram, A. Tam, C. D. Teemer, C. Thaller, C. L. Thompson, L. R. Varnam, A. Visel, R. M. Whitlock, P. E. Wohnoutka, C. K. Wolkey, V. Y. Wong, M. Wood, M. B. Yaylaoglu, R. C. Young, B. L. Youngstrom, X. F. Yuan, B. Zhang, T. A. Zwingman, A. R. Jones, Genome-wide atlas of gene expression in the adult mouse brain. *Nature* **445**, 168-176 (2007).
39. Y. Zhang, K. Chen, S. A. Sloan, M. L. Bennett, A. R. Scholze, S. O'Keeffe, H. P. Phatnani, P. Guarnieri, C. Caneda, N. Ruderisch, S. Deng, S. A. Liddelow, C. Zhang, R. Daneman, T. Maniatis, B. A. Barres, J. Q. Wu, An RNA-sequencing transcriptome and splicing database of glia, neurons, and vascular cells of the cerebral cortex. *J Neurosci* **34**, 11929-11947 (2014).
40. B. F. Verhaaren, S. Debette, J. C. Bis, J. A. Smith, M. K. Ikram, H. H. Adams, A. H. Beecham, K. B. Rajan, L. M. Lopez, S. Barral, M. A. van Buchem, J. van der Grond, A. V. Smith, K. Hegenscheid, N. T. Aggarwal, M. de Andrade, E. J. Atkinson, M. Beekman, A. S. Beiser, S. H. Blanton, E. Boerwinkle, A. M. Brickman, R. N. Bryan, G. Chauhan, C. P. Chen, V. Chouraki, A. J. de Craen, F. Crivello, I. J. Deary, J. Deelen, P. L. De Jager, C. Dufouil, M. S. Elkind, D. A. Evans, P. Freudenberger, R. F. Gottesman, V. Guethnason, M. Habes, S. R. Heckbert, G. Heiss, S. Hilal, E. Hofer, A. Hofman, C. A. Ibrahim-Verbaas, D. S. Knopman, C. E. Lewis, J. Liao, D. C. Liewald, M. Luciano, A. van der Lugt, O. O. Martinez, R. Mayeux, B. Mazoyer, M. Nalls, M. Nauck, W. J. Niessen, B. A. Oostra, B. M. Psaty, K. M. Rice, J. I. Rotter, B. von Sarnowski, H. Schmidt, P. J. Schreiner, M. Schuur, S. S. Sidney, S. Sigurdsson, P. E. Slagboom, D. J. Stott, J. C. van Swieten, A. Teumer, A. M. Toglhofer, M. Traylor, S. Trompet, S. T. Turner, C. Tzourio, H. W. Uh, A. G. Uitterlinden, M. W. Vernooij, J. J. Wang, T. Y. Wong, J. M. Wardlaw, B. G. Windham, K. Wittfeld, C. Wolf, C. B. Wright, Q. Yang, W. Zhao, A. Zijdenbos, J. W. Jukema, R. L. Sacco, S. L. Kardia, P. Amouyel, T. H. Mosley, W. T. Longstreth, Jr., C. C. DeCarli, C. M. van Duijn, R. Schmidt, L. J. Launer, H. J. Grabe, S. S. Seshadri, M. A. Ikram, M. Fornage, Multiethnic genome-wide association study of cerebral white matter hyperintensities on MRI. *Circ Cardiovasc Genet* **8**, 398-409 (2015).
41. D. R. Nyholt, A simple correction for multiple testing for single-nucleotide polymorphisms in linkage disequilibrium with each other. *Am J Hum Genet* **74**, 765-769 (2004).
42. E. V. Backhouse, C. A. McHutchison, V. Cvoro, S. D. Shenkin, J. M. Wardlaw, Early life risk factors for cerebrovascular disease: A systematic review and meta-analysis. *Neurology* **88**, 976-984 (2017).
43. K. Ozaki, T. Hori, T. Ishibashi, M. Nishio, Y. Aizawa, Effects of chronic cigarette smoking on endothelial function in young men. *J Cardiol* **56**, 307-313 (2010).

44. M. T. Johnstone, S. J. Creager, K. M. Scales, J. A. Cusco, B. K. Lee, M. A. Creager, Impaired endothelium-dependent vasodilation in patients with insulin-dependent diabetes mellitus. *Circulation* **88**, 2510-2516 (1993).
45. J. A. Panza, A. A. Quyyumi, J. E. Brush, Jr., S. E. Epstein, Abnormal endothelium-dependent vascular relaxation in patients with essential hypertension. *N Engl J Med* **323**, 22-27 (1990).
46. A. Poggesi, M. Pasi, F. Pescini, L. Pantoni, D. Inzitari, Circulating biologic markers of endothelial dysfunction in cerebral small vessel disease: A review. *J Cereb Blood Flow Metab* **36**, 72-94 (2016).
47. S. F. Stevenson, F. N. Doubal, K. Shuler, J. M. Wardlaw, A systematic review of dynamic cerebral and peripheral endothelial function in lacunar stroke versus controls. *Stroke* **41**, e434-442 (2010).
48. A. Joutel, M. Monet-Lepretre, C. Gosele, C. Baron-Menguy, A. Hammes, S. Schmidt, B. Lemaire-Carrette, V. Domenga, A. Schedl, P. Lacombe, N. Hubner, Cerebrovascular dysfunction and microcirculation rarefaction precede white matter lesions in a mouse genetic model of cerebral ischemic small vessel disease. *J Clin Invest* **120**, 433-445 (2010).
49. T. Van Agtmael, M. A. Bailey, U. Schlotzer-Schrehardt, E. Craigie, I. J. Jackson, D. G. Brownstein, I. L. Megson, J. J. Mullins, Col4a1 mutation in mice causes defects in vascular function and low blood pressure associated with reduced red blood cell volume. *Hum Mol Genet* **19**, 1119-1128 (2010).
50. A. Elbaz, O. Poirier, T. Moulin, F. Chedru, F. Cambien, P. Amarenco, Association between the Glu298Asp polymorphism in the endothelial constitutive nitric oxide synthase gene and brain infarction. The GENIC Investigators. *Stroke* **31**, 1634-1639 (2000).
51. A. Hassan, K. Gormley, M. O'Sullivan, J. Knight, P. Sham, P. Vallance, J. Bamford, H. Markus, Endothelial nitric oxide gene haplotypes and risk of cerebral small-vessel disease. *Stroke* **35**, 654-659 (2004).
52. X. Tang, M. S. Halleck, R. A. Schlegel, P. Williamson, A subfamily of P-type ATPases with aminophospholipid transporting activity. *Science* **272**, 1495-1497 (1996).
53. M. Moreno-Smith, J. B. Halder, P. S. Meltzer, T. A. Gonda, L. S. Mangala, R. Rupaimoole, C. Lu, A. S. Nagaraja, K. M. Gharpure, Y. Kang, C. Rodriguez-Aguayo, P. E. Vivas-Mejia, B. Zand, R. Schmandt, H. Wang, R. R. Langley, N. B. Jennings, C. Ivan, J. E. Coffin, G. N. Armaiz, J. Bottsford-Miller, S. B. Kim, M. S. Halleck, M. J. Hendrix, W. Bornman, M. Bar-Eli, J. S. Lee, Z. H. Siddik, G. Lopez-Berestein, A. K. Sood, ATP11B mediates platinum resistance in ovarian cancer. *J Clin Invest* **123**, 2119-2130 (2013).
54. Q. Zhang, J. E. Church, D. Jagnandan, J. D. Catravas, W. C. Sessa, D. Fulton, Functional relevance of Golgi- and plasma membrane-localized endothelial NO synthase in reconstituted endothelial cells. *Arterioscler Thromb Vasc Biol* **26**, 1015-1021 (2006).
55. S. Sato, N. Fujita, T. Tsuruo, Modulation of Akt kinase activity by binding to Hsp90. *Proc Natl Acad Sci U S A* **97**, 10832-10837 (2000).
56. A. I. Flores, B. S. Mallon, T. Matsui, W. Ogawa, A. Rosenzweig, T. Okamoto, W. B. Macklin, Akt-mediated survival of oligodendrocytes induced by neuregulins. *J Neurosci* **20**, 7622-7630 (2000).
57. C. R. Sussman, T. Vartanian, R. H. Miller, The ErbB4 neuregulin receptor mediates suppression of oligodendrocyte maturation. *J Neurosci* **25**, 5757-5762 (2005).
58. T. J. Yuen, J. C. Silbereis, A. Griveau, S. M. Chang, R. Daneman, S. P. J. Fancy, H. Zahed, E. Maltepe, D. H. Rowitch, Oligodendrocyte-encoded HIF function couples postnatal myelination and white matter angiogenesis. *Cell* **158**, 383-396 (2014).
59. D. A. Mayes, T. A. Rizvi, H. Titus-Mitchell, R. Oberst, G. M. Ciraolo, C. V. Vorhees, A. P. Robinson, S. D. Miller, J. A. Cancelas, A. O. Stemmer-Rachamimov, N. Ratner, Nf1 loss and Ras hyperactivation in oligodendrocytes induce NOS-driven defects in myelin and vasculature. *Cell Rep* **4**, 1197-1212 (2013).
60. H. H. Tsai, J. Niu, R. Munji, D. Davalos, J. Chang, H. Zhang, A. C. Tien, C. J. Kuo, J. R. Chan, R. Daneman, S. P. Fancy, Oligodendrocyte precursors migrate along vasculature in the developing nervous system. *Science* **351**, 379-384 (2016).
61. K. Arai, E. H. Lo, An oligovascular niche: cerebral endothelial cells promote the survival and proliferation of oligodendrocyte precursor cells. *J Neurosci* **29**, 4351-4355 (2009).

62. R. M. Rajani, A. Williams, Endothelial cell-oligodendrocyte interactions in small vessel disease and aging. *Clin Sci (Lond)* **131**, 369-379 (2017).
63. C. Valdes Hernandez Mdel, T. Booth, C. Murray, A. J. Gow, L. Penke, Z. Morris, S. M. Maniega, N. A. Royle, B. S. Aribisala, M. E. Bastin, J. M. Starr, I. J. Deary, J. M. Wardlaw, Brain white matter damage in aging and cognitive ability in youth and older age. *Neurobiol Aging* **34**, 2740-2747 (2013).
64. J. M. Wardlaw, M. C. Valdes Hernandez, S. Munoz-Maniega, What are white matter hyperintensities made of? Relevance to vascular cognitive impairment. *J Am Heart Assoc* **4**, 001140 (2015).
65. J. H. Fu, V. Mok, W. Lam, A. Wong, W. Chu, Y. Xiong, P. W. Ng, T. H. Tsoi, V. Yeung, K. S. Wong, Effects of statins on progression of subclinical brain infarct. *Cerebrovasc Dis* **30**, 51-56 (2010).
66. C. Dufouil, J. Chalmers, O. Coskun, V. Besancon, M. G. Bousser, P. Guillon, S. MacMahon, B. Mazoyer, B. Neal, M. Woodward, N. Tzourio-Mazoyer, C. Tzourio, P. M. S. Investigators, Effects of blood pressure lowering on cerebral white matter hyperintensities in patients with stroke: the PROGRESS (Perindopril Protection Against Recurrent Stroke Study) Magnetic Resonance Imaging Substudy. *Circulation* **112**, 1644-1650 (2005).
67. H. M. Vesterinen, E. S. Sena, C. ffrench-Constant, A. Williams, S. Chandran, M. R. Macleod, Improving the translational hit of experimental treatments in multiple sclerosis. *Mult Scler* **16**, 1044-1055 (2010).
68. N. H. Anderson, A. M. Devlin, D. Graham, J. J. Morton, C. A. Hamilton, J. L. Reid, N. J. Schork, A. F. Dominiczak, Telemetry for cardiovascular monitoring in a pharmacological study: new approaches to data analysis. *Hypertension* **33**, 248-255 (1999).
69. H. Edrissi, S. C. Schock, R. Cadonic, A. M. Hakim, C. S. Thompson, Cilostazol reduces blood brain barrier dysfunction, white matter lesion formation and motor deficits following chronic cerebral hypoperfusion. *Brain Res* **1646**, 494-503 (2016).
70. H. H. Koh-Tan, D. Graham, C. A. Hamilton, G. Nicoll, L. Fields, M. W. McBride, B. Young, A. F. Dominiczak, Renal and vascular glutathione S-transferase mu is not affected by pharmacological intervention to reduce systolic blood pressure. *J Hypertens* **27**, 1575-1584 (2009).
71. H. Zhang, A. A. Jarjour, A. Boyd, A. Williams, Central nervous system remyelination in culture--a tool for multiple sclerosis research. *Exp Neurol* **230**, 138-148 (2011).
72. G. Levi, H. Meyer, Nouvelles recherches sur le tissu nerveux cultivé in vitro. Morphologie, croissance et relations réciproques des neurones. *Arch. Biol.(Paris)* **52**, 133-278 (1941).
73. N. J. Abbott, C. C. Hughes, P. A. Revest, J. Greenwood, Development and characterisation of a rat brain capillary endothelial culture: towards an in vitro blood-brain barrier. *J Cell Sci* **103 (Pt 1)**, 23-37 (1992).
74. K. D. McCarthy, J. de Vellis, Preparation of separate astroglial and oligodendroglial cell cultures from rat cerebral tissue. *J Cell Biol* **85**, 890-902 (1980).
75. W. Li, Y. Li, S. Guan, J. Fan, C. F. Cheng, A. M. Bright, C. Chinn, M. Chen, D. T. Woodley, Extracellular heat shock protein-90alpha: linking hypoxia to skin cell motility and wound healing. *EMBO J* **26**, 1221-1233 (2007).
76. N. K. Acharya, E. L. Goldwaser, M. M. Forsberg, G. A. Godsey, C. A. Johnson, A. Sarkar, C. DeMarshall, M. C. Kosciuk, J. M. Dash, C. P. Hale, D. M. Leonard, D. M. Appelt, R. G. Nagele, Sevoflurane and Isoflurane induce structural changes in brain vascular endothelial cells and increase blood-brain barrier permeability: Possible link to postoperative delirium and cognitive decline. *Brain Res* **1620**, 29-41 (2015).
77. A. B. Nair, S. Jacob, A simple practice guide for dose conversion between animals and human. *J Basic Clin Pharm* **7**, 27-31 (2016).

Acknowledgments: We thank the MRC Edinburgh Sudden Death Brain Bank for providing human brain tissue, and CHARGE for the provision of SNP data. We also thank M. Swire and C. ffrench-Constant for providing us with the bEND.3 cell line, E. Beattie for assistance with in vivo work, Bertrand Vernay and Max Ahmed for help with imaging, and V. Miron for commenting on an earlier draft of this manuscript.

Funding: This work was supported by the UK Medical Research Council, Alzheimer's Research UK, Fondation Leducq (16 CVD 05) and the BHF Centre for Research Excellence (RE/13/5/30177). The University of Edinburgh Centre for Cognitive Ageing and Cognitive Epidemiology supports SEH and is funded by the MRC and BBSRC (grant No. MR/K026992/1).

Author contributions: R.M.R designed, carried out and analyzed most of the experiments, and wrote the manuscript. S.Q. carried out the human endothelial cell work, ELISAs, tracer experiments and some western blots. S.R.R. carried out the conditioned media experiments on slices and assisted with the rat sequencing. D.G. and A.F.D. provided the SHRSP and WKY rats, and D.G. carried out the perfusions and assisted with the drug study. B.F.J.V, M.F. and S.S. provided the SNP summary data, and S.E.H. carried out the multiple testing correction. S.S.A. provided advice on reanalysis of the rat gene array data. C.S. and J.M.W co-supervised the project and assisted in study design. J.M.W. initiated the original experiments, added important context, and assisted in data interpretation and editing of the manuscript. A.W. supervised the project, and assisted in study design, data interpretation and writing of the manuscript. All authors assisted with editing of the manuscript.

Competing interests: The authors declare no competing financial interests.

Data and materials availability: All relevant data are available in the manuscript and the Supplementary Materials. Requests for materials should be addressed to A.W. (anna.williams@ed.ac.uk).

Fig. 1. Pathological changes to the BBB and OPCs in brains of young DM rats and pre-symptomatic humans. A-H: Immunofluorescent images from brain deep white matter and graph (**I**) showing number of blood vessels (CD34+; red) with claudin-5 positive tight junctions (TJs; green) in the DM rats (**B**, **D**) compared to controls (**A**, **C**), and in diseased human brains (**F**, **H**) compared to controls (**E**, **G**). Arrows indicate blood vessels without claudin-5 positive TJs. **C**, **D**, **G**, **H** show enlarged images of the white boxes in **A**, **B**, **E**, **F** respectively. **J-O:** Number of OPCs ($Olig2^+Nogo\text{-}A^-$; indicated by arrows) per mm^2 (**J-N**) and mature oligodendrocytes ($Olig2^+Nogo\text{-}A^+$) **(K-O)** in DM rats and in diseased human brains compared to controls (Olig2, all oligodendroglia, green; Nogo-A, mature oligodendrocytes, red). **(P)** Number of proliferating OPCs ($Olig2^+$ $PCNA^+$) per mm^2 in the DM rats and in the diseased human brains compared to controls. (Mean ± SEM; $^{**}P<0.01$, $^{*}P<0.05$, two-way ANOVA with Tukey's post-hoc tests; 3wk: n≥4 animals; 4wk: n≥3 animals; 5wk: **P**: n=3, others: n=10 animals; human: n=5). Scale bars = 25 μm.

Fig. 2. Endothelial cells are dysfunctional at 3 weeks of age in DM rats and in human brains with SVD. A-F: Slice data demonstrating early changes are not due to blood brain barrier leakage. **A-B**: Western blot and quantification of claudin-5 in brain slices cultured from DM rats for 5 weeks compared to controls ($^{*}P<0.05$, paired t-test; n=3 experiments). GAPDH is the loading control. **C-F** Immunofluorescent images and quantification of brain slices stained for Olig2 (all oligodendroglia; green), and Nogo-A (mature oligodendrocytes; red) in DM rat slices (**D**) compared to control (**C**) ($^{*}P<0.05$, paired t-test; n=5 experiments). **G-H**: Western blot and quantification of eNOS in 3-week-old DM rat brain tissue compared to controls (Ctrl), with GAPDH as a loading control ($^{*}P<0.05$, unpaired t-test; n=3 animals). **I-J**: Immunofluorescent images showing proliferating ($PCNA^+$; red) endothelial cells ($CD34^+$; green) (indicated by white arrows) in the deep white matter of brains from 3-week-old control (**I**) and DM rats (**J**). Enlargements of boxed areas shown. **K-L**: Colorimetric immunostaining of proliferating ($PCNA^+$; blue) human ECs ($CD34^+$; brown) (red arrows). **M**: Quantification of the number of proliferating ECs per mm^2 in the DM rat brains and the diseased human brains compared to their controls. (Mean ± SEM; $^{*}P<0.05$, $^{**}P<0.01$, $^{***}P<0.001$, $^{****}P<0.0001$, two-way ANOVA with Tukey's post-hoc tests; 3wk: n=5 animals; 4wk, 5wk: n=3 animals; human: n=5). **N**: Assay of nitrates and nitrites (NO_x) as a proxy for cell production of nitric oxide in the media of BMECs isolated from DM rats compared to controls. Each color represents a different paired repeat (Mean ± SEM; $^{*}P<0.05$, paired t-test; n=3 BMEC preparations from different litters). **O-P**:

Immunofluorescent staining showing claudin-5 (mature TJ protein; green) and ZO-1 (immature TJ protein; red) in BMEC cultures isolated from control (**O**) and DM (**P**) rats, quantified in (**Q-R**) (*P<0.05, paired t-test; n=3 BMEC preparations from different litters). (Hoechst, blue). Scale bar = 25 μm.

Fig. 3. HSP90α produced by BMECs reduces OPC maturation. A-B: Immunofluorescent images showing OPCs ($NG2^+$; green), and MBP-expressing mature oligodendrocytes (red), in cultures grown in disease model (DM) (**B**) compared to control (**A**) BMEC conditioned media (CM) (*P<0.05, paired t-test; n=3 experiments, quantified in **C,D**). **E-F**: Proliferating Ki67-expressing cells (red) in cultures of OPCs grown in DM (**F**) compared to control (**E**) BMEC CM (*P<0.05, paired t-test; n=3 experiments, quantified in **G**). **H-J**: OPCs [$Olig2^+$ (all oligodendroglia; green) $Nogo\text{-}A^-$ (mature oligodendrocytes; red), arrows indicating $Olig2^+NogoA^-$ OPCs] in wild type brain slices grown in culture for 5 weeks in DM BMEC CM (**J**) compared to control CM (**I**) (Quantified in **H** normalized to slices grown in in unconditioned media; *P<0.05, paired t-test; n=3 experiments). **K**: Western blot for HSP90α in CM from DM BMECs compared to controls (*P<0.05, paired t-test; n=3 experiments, quantified in **L**), including Ponceau stain of membrane showing total protein as loading control, with prominent band of bovine serum albumin. **M**: ELISA for HSP90α in CM from DM BMECs compared to controls (P=0.05, t-test; n=4 experiments). **N-Q**: Effect of addition of recombinant (r)HSP90α on maturation of wild type OPCs in culture (immature $NG2^+$ OPCs, green; mature MBP^+ oligodendrocytes, red) (Quantified in **P-Q** with each color representing a different paired repeat; *P<0.05, paired t-test; n=4 experiments). **R-V**: Effect of addition of HSP90α blocking antibody (BA) on OPC cultures grown in DM CM (immature $NG2^+$ OPCs, green; mature MBP^+ oligodendrocytes, red). **U-V:** Quantification of the percentage of $NG2^+$ cells is normalized to control CM (such that 1 = an average of 23% $NG2^+$) and quantification of the percentage of MBP^+ cells is normalized to control CM (such that 1 = an average of 15% MBP^+). (Mean ± SEM; *P<0.05, **P<0.01, 1-way repeated measures ANOVA with Bonferroni post-hoc tests; n=4 separate experiments with cells from different litters). **W**: Western blot showing full-length and cleaved, secreted forms of HSP90α (with GAPDH as loading control) in rat and human control and diseased brains [*P<0.05, unpaired t-test; n=3 rats each group quantified in (**X**); P=0.28, unpaired t-test; n=5 humans each group quantified in (**Y**)]. Scale bar = 25 μm. Hoechst (blue).

Fig. 4. Drugs which reduce EC dysfunction also reduce white matter vulnerability. A: Timeline of drug trial, showing the ages at which pathologies appear, the timing of blood

pressure measurements, and the beginning and end of treatment. **B**: Table of treatment groups and effects. All drugs were administered daily through an oral route at the following concentrations: simvastatin: 2 mg/kg; perindopril: 2 mg/kg; cilostazol: 60 mg/kg; H+H: 16 mg/kg of each. **C**: Blood pressure readings over experiment. **D-K**: Immunofluorescence images showing the effect of simvastatin on EC proliferation, mature tight junctions, OPC and oligodendrocyte numbers and OPC proliferation, with quantification in graphs (**L-P**). **Q**: Blinded ranking of myelin rarefaction on Luxol blue/Cresyl violet stained brain sections. (Mean ± SEM; **P*<0.05, ***P*<0.01, ****P*<0.001, **L-P**: 1-way ANOVA with Bonferroni post-hoc tests, **Q**: Kruskal-Wallis test with Dunn's post-hoc tests; cilostazol: n=4, others: n=5 animals per treatment group.) Scale bar = 25 μm.

Fig. 5. *Atp11b* is mutated in disease model rats and leads to dysfunctional ECs. A: Filtering strategy: Venn diagram with overlap of genes with frameshift or STOP-gain mutations in the stroke-prone spontaneously hypertensive rat (SHRSP) and the spontaneously hypertensive rat (SHR). Mutations unique to SHRSP were filtered first using Variant Effect Predictor (Ve!P) tool from ENSEMBL (*37*) to select those predicted to lead to truncated proteins, then with the Allen Mouse Brain Atlas (*38*) to select genes expressed in the brain and finally with the Barres Brain RNA-Seq database (*39*) to select genes expressed in brain ECs. **B**: DNA sequence showing the 28 base pair deletion in the *Atp11b* gene, and corresponding cDNA. **C**: Western blot with complete loss of ATP11B in the DM rat brains compared to controls, using an N-terminus antibody. **D**: Western blot of knock-down of ATP11B in bEND.3 cells treated with *Atp11b* siRNA (*Atp11b*-KD) compared with non-targeting siRNA (control) (**P*<0.05, paired t-test; n=3 experiments, quantified in **E**; GAPDH=loading control). **F-G:** Immunofluorescent images showing proliferation ($Ki67^+$ nuclei; magenta; white arrows) in *Atp11b*-KD bEND.3 cells (**G**) compared to controls (**F**) (quantified in **H**; **P*<0.05, paired t-test; n=3 experiments). **I-L**: Immunofluorescent images staining for claudin-5 (mature TJ protein; green) compared to ZO-1 (immature TJ protein; red) in *Atp11b*-KD bEND.3 cells (**J**) compared to controls (**I**) (quantified in **K-L**; **P*<0.05, paired t-test; n=3 experiments). **M-P**: Differentiation of OPCs ($NG2^+$ immature OPCs, green; MBP^+ mature oligodendrocytes, red) cultured in either conditioned media (CM) from *Atp11b*-KD bEND.3 cells (**N**) or control cells (**M**) (quantified in **O-P**; **P*<0.05, paired t-test; n=4 experiments). **Q-S**: Proliferation ($Ki67^+$; red) of OPCs cultured in CM from *Atp11b*-KD bEND.3 cells (**R**) compared to controls (**Q**), quantified in S (**P*<0.05, paired t-test; n=3 experiments). **T**: Western blot of HSP90α in CM from *Atp11b*-KD bEND.3 cells compared to controls (quantified in **U**; *: *P*<0.05, paired t-test; n=3 experiments), including

Ponceau stain of the membrane, showing total protein (prominent band is bovine serum albumin) as loading control. Scale bar = 25 μm. Hoechst=blue.

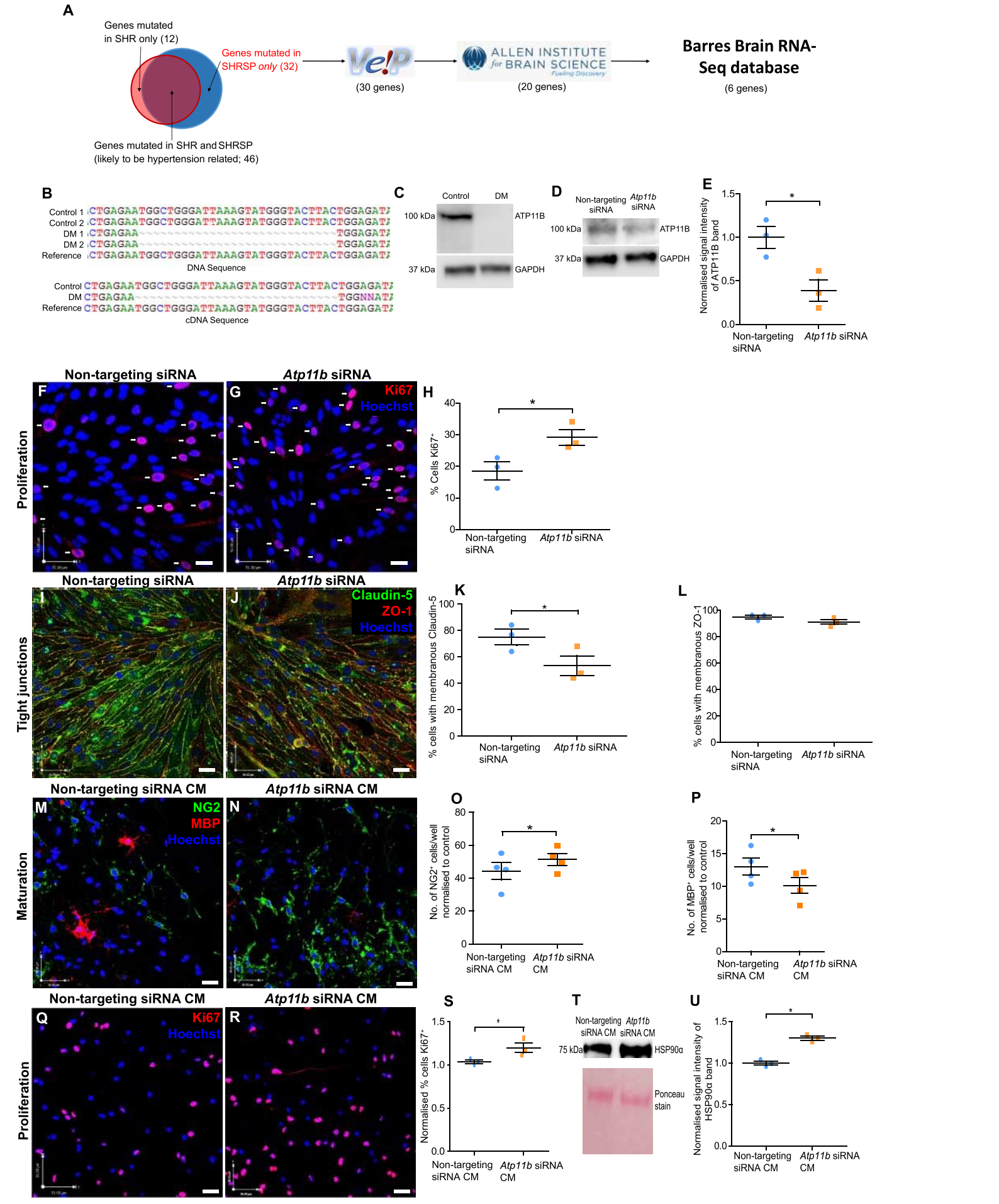
A
Genes mutated in SHR only (12)
Genes mutated in SHRSP only (32)
Genes mutated in SHR and SHRSP (likely to be hypertension related; 46)
(30 genes)
(20 genes)
Barres Brain RNA-Seq database
(6 genes)
B
Control 1
Control 2
DM 1
DM 2
Reference
DNA Sequence
cDNA Sequence
C
Control
DM
100 kDa
ATP11B
37 kDa
GAPDH
D
Non-targeting siRNA
Atp11b siRNA
E
Normalised signal intensity of ATP11B band
Non-targeting siRNA
Atp11b siRNA
Non-targeting siRNA
Atp11b siRNA
Proliferation
F
G
Ki67
Hoechst
H
% Cells Ki67+
Tight junctions
I
J
Claudin-5
ZO-1
K
% cells with membranous Claudin-5
L
% cells with membranous ZO-1
Non-targeting siRNA CM
Atp11b siRNA CM
Maturation
M
N
NG2
MBP
O
No. of NG2+ cells/well normalised to control
P
No. of MBP+ cells/well normalised to control
Q
R
S
Normalised % cells Ki67+
T
75 kDa
HSP90α
Ponceau stain
U
Normalised signal intensity of HSP90α band

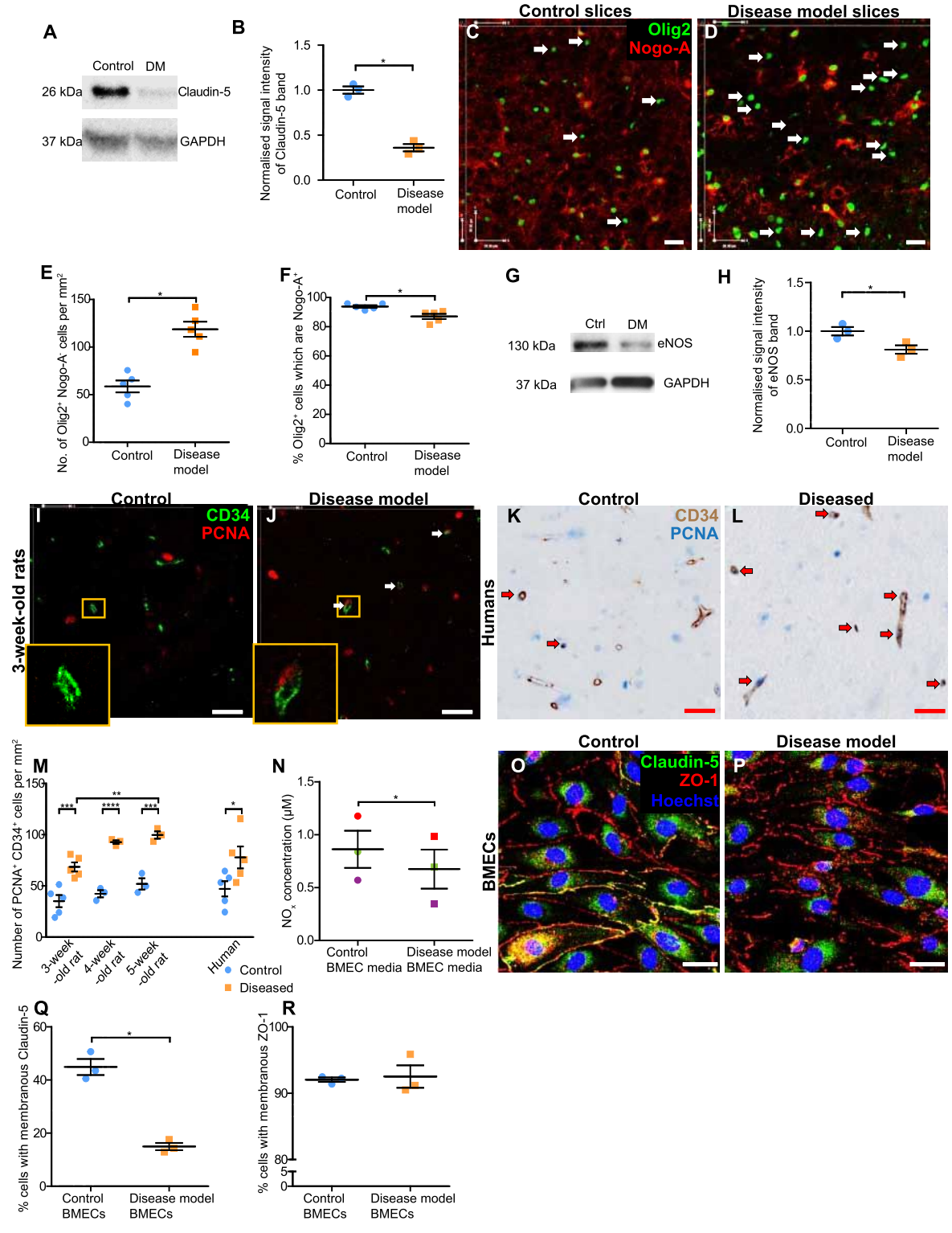
A
Control
DM
26 kDa
Claudin-5
37 kDa
GAPDH
B
Normalised signal intensity of Claudin-5 band
Control
Disease model
Control slices
Disease model slices
C
Olig2
Nogo-A
D
E
No. of Olig2+ Nogo-A- cells per mm2
F
% Olig2+ cells which are Nogo-A+
G
Ctrl
DM
130 kDa
eNOS
37 kDa
GAPDH
H
Normalised signal intensity of eNOS band
I
CD34
PCNA
3-week-old rats
J
K
Humans
L
M
Number of PCNA+ CD34+ cells per mm2
3-week -old rat
4-week -old rat
5-week -old rat
Human
Control
Diseased
N
NOx concentration (μM)
Control BMEC media
Disease model BMEC media
O
Claudin-5
ZO-1
Hoechst
BMECs
P
Q
% cells with membranous Claudin-5
Control BMECs
Disease model BMECs
R
% cells with membranous ZO-1

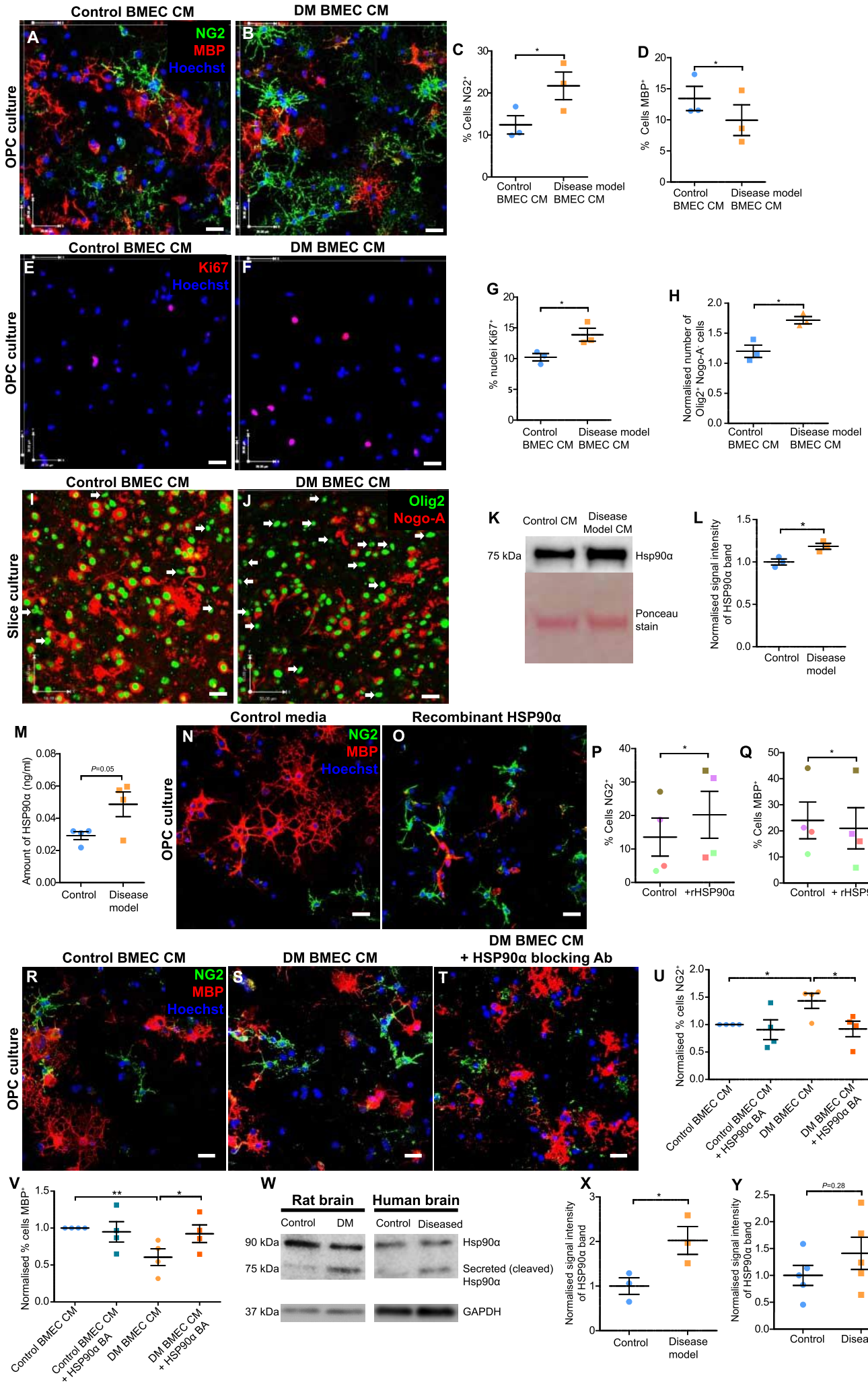
Control BMEC CM
DM BMEC CM
OPC culture
A
B
NG2
MBP
Hoechst
C
% Cells NG2+
Control BMEC CM
Disease model BMEC CM
D
% Cells MBP+
Control BMEC CM
Disease model BMEC CM
Control BMEC CM
DM BMEC CM
OPC culture
E
F
Ki67
Hoechst
G
% nuclei Ki67+
Control BMEC CM
Disease model BMEC CM
H
Normalised number of Olig2+ Nogo-A- cells
Control BMEC CM
Disease model BMEC CM
Control BMEC CM
DM BMEC CM
Slice culture
I
J
Olig2
Nogo-A
K
Control CM
Disease Model CM
75 kDa
Hsp90α
Ponceau stain
L
Normalised signal intensity of HSP90α band
Control
Disease model
M
Amount of HSP90α (ng/ml)
P=0.05
Control
Disease model
Control media
Recombinant HSP90α
OPC culture
N
O
NG2
MBP
Hoechst
P
% Cells NG2+
Control
+rHSP90α
Q
% Cells MBP+
Control
+ rHSP90α
Control BMEC CM
DM BMEC CM
+ HSP90α blocking Ab
OPC culture
R
S
T
NG2
MBP
Hoechst
U
Normalised % cells NG2+
Control BMEC CM
Control BMEC CM + HSP90α BA
DM BMEC CM
DM BMEC CM + HSP90α BA
V
Normalised % cells MBP+
Control BMEC CM
Control BMEC CM + HSP90α BA
DM BMEC CM
DM BMEC CM + HSP90α BA
W
Rat brain
Human brain
Control
DM
Control
Diseased
90 kDa
75 kDa
Hsp90α
Secreted (cleaved) Hsp90α
37 kDa
GAPDH
X
Normalised signal intensity of HSP90α band
Control
Disease model
Y
P=0.28
Normalised signal intensity of HSP90α band
Control
Diseased

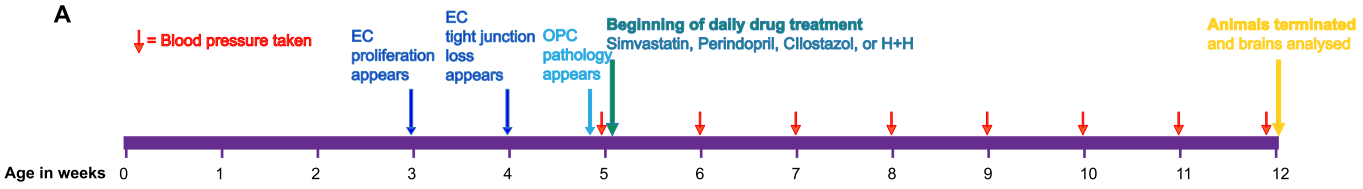

B

Symbol	Treatment group	Abbreviation	Reduces blood pressure	Improves EC dysfunction
●	Untreated Ctrl	UC	-	-
■	Untreated DM	UDM	-	-
▲	Simvastatin DM	SDM	-	✓
▼	Perindopril DM	PDM	✓	✓
●	Cilostazol DM	CDM	-	✓
◆	H+H DM	HDM	✓	-

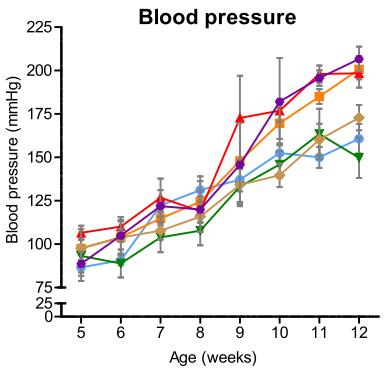

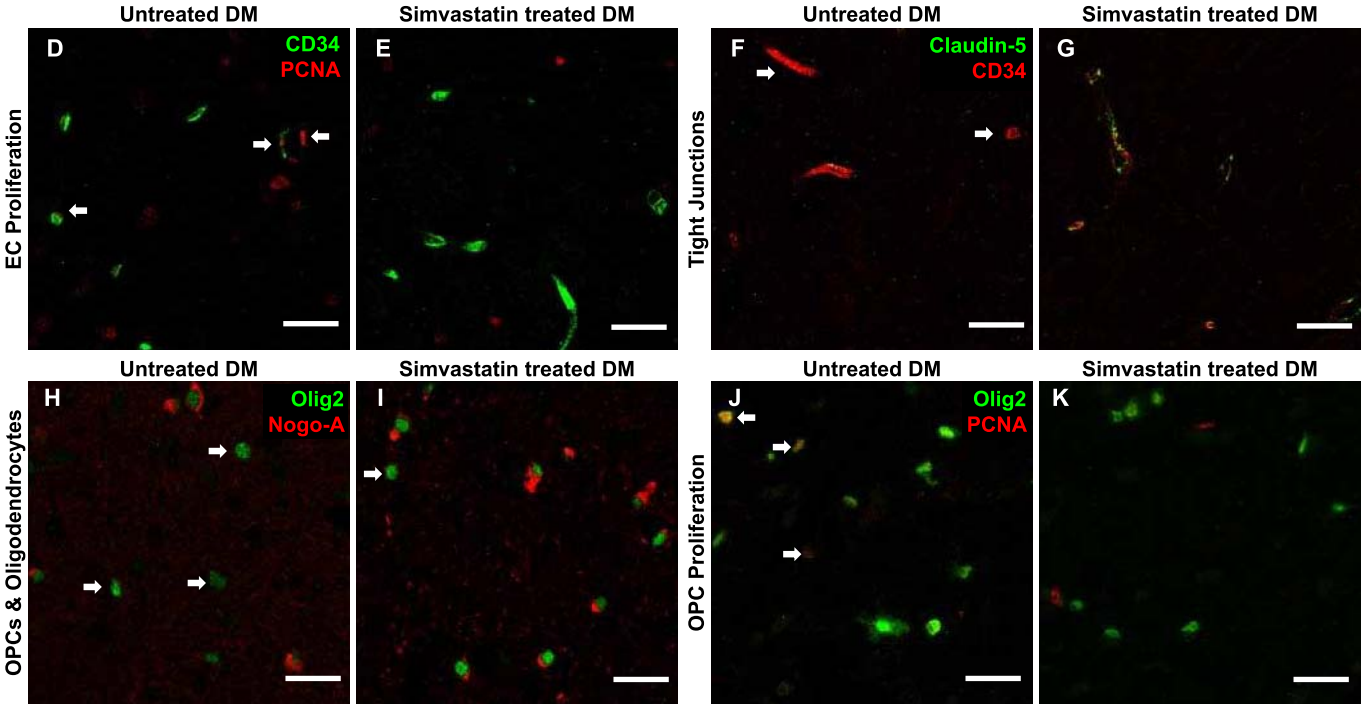

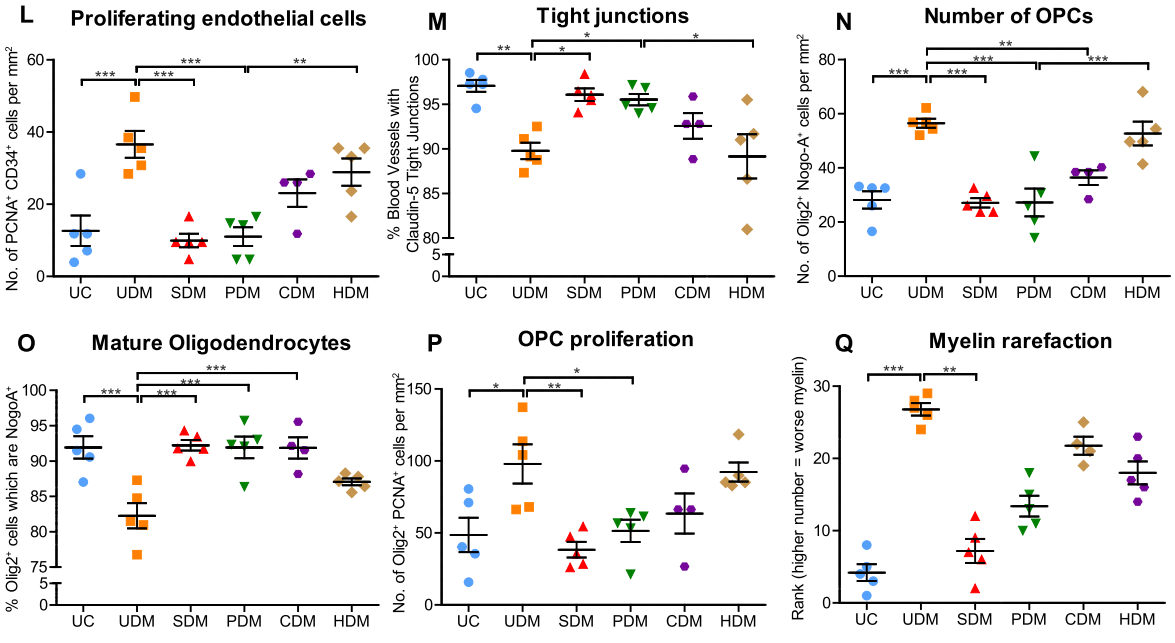

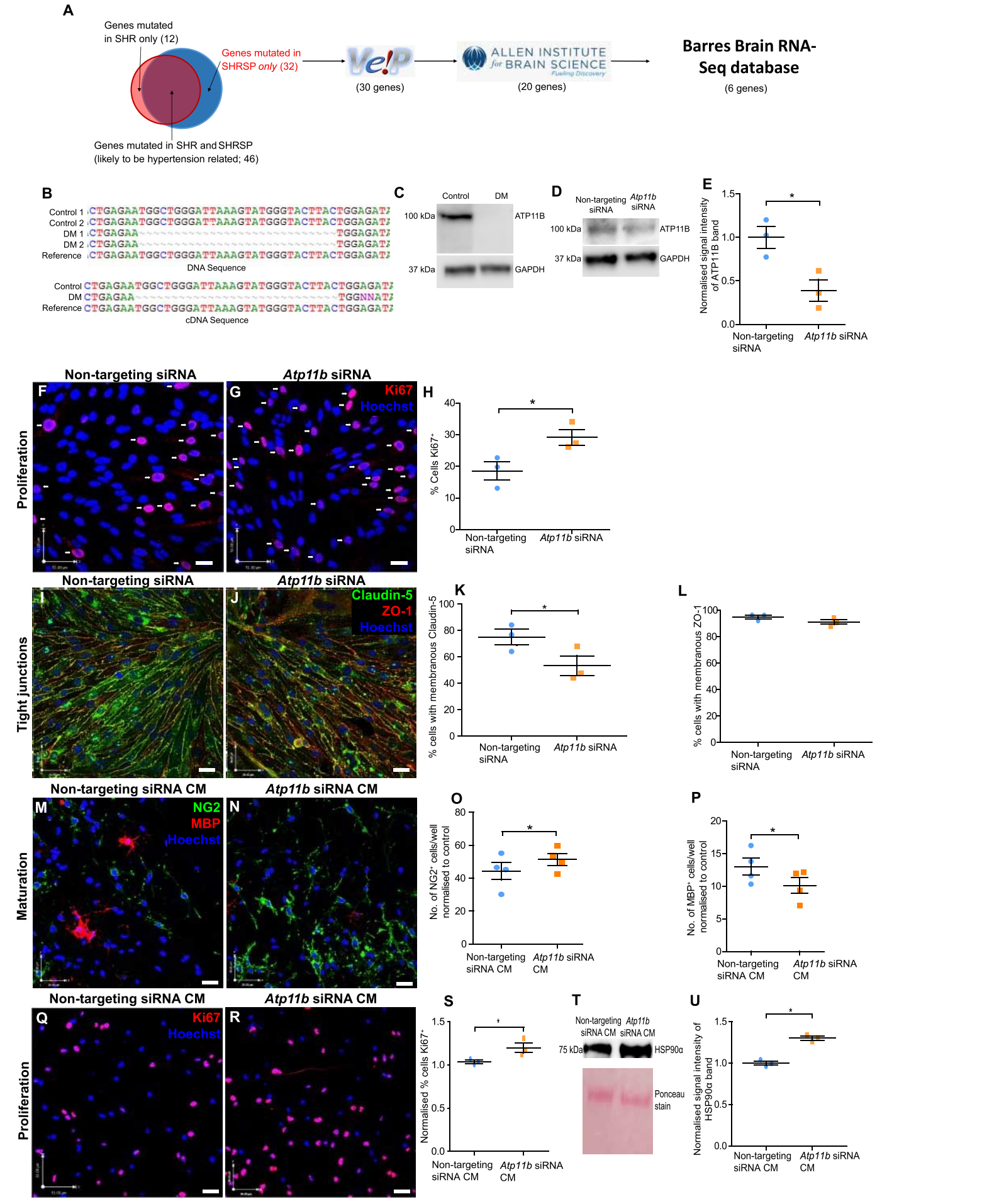
A
Genes mutated in SHR only (12)
Genes mutated in SHRSP only (32)
Genes mutated in SHR and SHRSP (likely to be hypertension related; 46)
(30 genes)
(20 genes)
Barres Brain RNA-Seq database
(6 genes)
B
Control 1
Control 2
DM 1
DM 2
Reference
DNA Sequence
cDNA Sequence
C
Control
DM
100 kDa
ATP11B
37 kDa
GAPDH
D
Non-targeting siRNA
Atp11b siRNA
E
Normalised signal intensity of ATP11B band
Non-targeting siRNA
Atp11b siRNA
Non-targeting siRNA
Atp11b siRNA
Proliferation
F
G
Ki67
Hoechst
H
% Cells Ki67+
Tight junctions
I
J
Claudin-5
ZO-1
K
% cells with membranous Claudin-5
L
% cells with membranous ZO-1
Non-targeting siRNA CM
Atp11b siRNA CM
Maturation
M
N
NG2
MBP
O
No. of NG2+ cells/well normalised to control
P
No. of MBP+ cells/well normalised to control
Q
R
S
Normalised % cells Ki67+
T
75 kDa
HSP90α
Ponceau stain
U
Normalised signal intensity of HSP90α band

Materials and Methods

Animal housing and husbandry. Stroke-prone spontaneously hypertensive rats (SHRSP) and matched control strain, Wistar Kyoto rats (WKY), were housed at the University of Glasgow. Animals were fed standard chow and housed in line with Home Office guidelines. Breeding SHRSP pairs regularly had their blood pressure tested to ensure maintenance of the colony's phenotype. Male animals were exclusively used for both WKY controls and SHRSPs as SHRSP males display a more severe phenotype. Sprague Dawley rats housed at the University of Edinburgh were used for wild-type oligodendrocyte precursor cells (OPCs) and slice cultures.

Protocols for animal termination. OPCs and slices: postnatal day 0-2 by an overdose of Euthatal (150 mg/kg; Merial) administered intraperitoneally. Brain microvascular endothelial cells (BMECs): postnatal day 5-10 by a rising concentration of carbon dioxide (CO_2), as anesthetics can affect endothelial cell function (*76*). Extraction of protein lysates where fresh, frozen tissue was required: age of 5 weeks by an overdose of Euthatal (150 mg/kg) and brains extracted and flash frozen in liquid nitrogen. Immunohistochemistry (IHC): 3, 4 and 5 weeks of age by overdose of Euthatal (150 mg/kg) and intracardiac perfusion fixation with 4% paraformaldehyde (PFA; Sigma-Aldrich; diluted in phosphate buffered saline (PBS; Gibco)). Drug study: 12 weeks of age by overdose of inhaled Isoflurane (5%; Zoetis) plus intracardiac perfusion with heparinized (5 U/ml; Wockhardt) PBS, then 4% PFA.

Tracer experiments. In 5 week old animals 5% isoflurane in 1.5 l/min oxygen was used as anesthetic for intravenous injection of tracer mix (20 mg/ml Tetramethylrhodamine isothiocyanate-Dextran (Sigma-Aldrich T1162) (65-85 kD) in PBS). Animals were allowed to recover for 10 minutes before euthanizing with CO_2.

Preparation of tissue. IHC: brains were extracted from animals after perfusion fixation and incubated overnight in 4% PFA at 4°C, followed by an overnight incubation in 50% ethanol (VWR). Brains were

then processed for paraffin embedding by immersion in increasing concentrations of ethanol before being embedded in paraffin wax for sectioning at 4 μm. Tracer experiments: brains were extracted from animals after perfusion fixation and incubated overnight in 4% PFA at 4°C, followed by incubations in 30% sucrose (overnight, 4°C; Sigma-Aldrich) and 50% sucrose (overnight, 4°C). Brains were then embedded in optimal cutting temperature compound (OCT; CellPath) and frozen on dry ice. Sections were cut at 8 μm thickness using a cryostat.

Preparation and maintenance of cells

Preparation of brain slices. As adapted from a previously published method (*71, 72*). Brains were extracted from rats aged postnatal day 0-2, divided into hemispheres and trimmed to leave only mid-coronal regions (approximately Bregma +1 to Bregma -4) in L-15 medium (Sigma-Aldrich). This was placed onto a McIlwain Tissue Chopper to cut 300 μm thick coronal sections, teased apart, and plated on Millipore cell culture inserts (2-4 slices per insert) in 6-well plates with 1 ml slice culture medium [minimum essential medium (MEM; Gibco) with 25% Earle's balanced salt solution (EBSS; Gibco), 25% heat inactivated horse serum (HIHS; Gibco), 1.5% glucose (45%; Sigma-Aldrich), 1% glutamax (Gibco), 1% penicillin/streptomycin (pen/strep; Gibco), 0.5% Fungizone (Invitrogen)] underneath the insert. Medium was changed every 2-3 days, and slices were kept in culture for up to 5 weeks.

Preparation of BMECs. As adapted from a previously published method (*73*). Brains were extracted from rats aged postnatal day 5-10 and divided into hemispheres with cerebellum removed in working buffer (Hank's balanced salt solution (HBSS; Life Technologies) with 0.5% bovine serum albumin [chromatographically purified; BSA (cp); First Link UK Ltd), 0.5% HEPES (Gibco), 0.5% pen/strep]. Meninges were removed before brains were homogenized in 5 ml working buffer with a Dounce tissue grinder. Homogenate was isolated from the buffer by centrifugation for 5 minutes at 1800 revolutions per minute (RPM) at 4°C. Blood vessel fragments were pelleted from this homogenate by centrifugation in 22% BSA (cp) for 15 minutes at 3000 RPM at 4°C. The pellet of blood vessel fragments was kept on ice in working buffer while the remainder was centrifuged again, for a total of 5 spins. Blood vessel fragments were pipetted onto an upside down 70 μm cell strainer to remove single cells then washed into a pooled

mixture with working buffer. This was spun down (5 minutes at 1800 RMP, 4°C) and the pellet then digested in 10 ml collagenase/dispase (1 mg/ml; Roche) and DNase I type IV (40 μg/ml; Sigma-Aldrich) for 45 minutes at 37°C. The resultant dissociated endothelial cells were washed in working buffer and plated at 500,000 cells/well on collagen IV and fibronectin (100 μg/ml and 50 μg/ml respectively; Sigma-Aldrich; overnight, 4°C) coated coverslips in a 24-well plate in 1 ml Endothelial Growth Media-2 Bullet Kit [EGM-2; Lonza; Endothelial basal media-2 with 2% Fetal Bovine Serum (FBS), 0.4% hFGF-beta, 0.1% hEGF, 0.1% VEGF, 0.1% R3-IGF-1, 0.1% Ascorbic acid, 0.1% Gentamycin/Amphotericin-B, 0.1% puromycin (Sigma-Aldrich; 5 mg/ml in Dulbecco's phosphate buffered saline (DPBS; Sigma-Aldrich)] and 0.04% hydrocortisone). Cells were grown in 5% carbon dioxide (CO_2) and medium was changed every 2-3 days. Cultures were used in experiments once they had regions of confluence (10-14 days) and were kept for up to 4 weeks. For conditioned media experiments, BMECs were kept in EGM-2 until they had regions of confluence before being grown in medium of the target cell type.

Maintenance of mouse brain endothelial cell line, bEND.3. Cells were initially obtained from ATCC (catalogue number: CRL-2299) and donated to us by the ffrench-Constant group. Mycoplasma-free cells were grown in PDL (5 μg/ml; 1 hour, 37°C) and matrigel (1:40 in water; Corning; 1 hour, 37°C) coated vented T75 flasks in culture medium (DMEM, 10% FBS, 1% pen/strep). The cells were plated at 1:10 of confluent density and split every week. To split the cells, they were first washed with DPBS and then incubated for 10 minutes at 37°C in TVP [1.3 mM ethylenediaminetetraacetic acid (EDTA; from BDH), 0.025% trypsin (Gibco), 1% chicken serum (Sigma-Aldrich) in DPBS]. The cells were then agitated and diluted in culture medium to stop the digestion, before being further diluted for splitting or plating. For experiments, cells were plated at 1:2 of confluent density on PDL and matrigel coated coverslips in 24-well plates as above.

Preparation of human endothelial cells. Human umbilical vein endothelial cells (HUVECs) (Lonza) were cultured in EGM2 media (Lonza) or Human Endothelial-SFM (Thermo) supplemented with 10% FCS, 10 μg/ml bFGF Recombinant Human Protein (Life Technologies), 10 μg/ml EGF Recombinant Human Protein (Life Technologies) and 40 μg/ml Fibronectin from human plasma (Sigma-Aldrich) for a maximum of five passages. Human cerebral endothelial cell lines from the HBEC5i and hCMEC/d3 lines

cultured immediately after purchase did not express the endothelial markers CD31 (PECAM-1) or CD144 (VE-Cadherin), possibly due to only later passage numbers being now available and so were abandoned (**fig. S9**). To check the endothelial cell marker expression, cells were harvested using Trypsin + 0.25% EDTA and suspended in PBS + 10% FCS at $1x10^6$ cells/ml, then incubated with antibodies for 30 minutes at 4°C to stain for surface markers (CD31-FITC, BD Pharmingen 557508, 1:100), (CD144-PerCYP.Cy5, BD Pharmingen 561566), (CD45-V450, BD Pharmingen 560368, 1:100). They were then washed three times in PBS + 2% FCS before sorting with the BD FACSAria Fusion flow cytometer and analyzed using FlowJo software.

Preparation of OPCs. As based on a previously published method (*74*). Brains were extracted from rats aged postnatal day 0-2 and cortices isolated in MEM. Meninges were removed then cortices were minced with fine scissors and digested in MEM with papain (1.2 U/ml; Worthington), L-cysteine (0.24 mg/ml; Sigma-Aldrich) and DNase I type IV (40 µg/ml) for 1 hour at 37°C. Cells were diluted in culture medium (Dulbecco's modified Eagle medium (DMEM; Gibco) with 10% FBS (Gibco), 1% pen/strep), spun down (5 minutes at 1000 RPM), then triturated gently with a 19-gauge needle followed by with a 23-gauge needle. Cells were resuspended in culture medium (1.5 brains in 10ml per flask) and grown in vented T75 flasks coated with poly-D-lysine (PDL; Sigma-Aldrich; 5 µg/ml in water; minimum 1 hour coating, 37°C) in 7.5% CO_2. 10-14 days after dissection, the vented cap of the flasks was sealed and the flasks were placed on an orbital shaker at 240 RPM at 37°C. After 1 hour the medium was removed (containing loosely attached microglia), fresh medium added, and the flask returned to the shaker for 16-18 hours. This medium was removed and plated on 10cm plastic petri dishes for 20-25 minutes (to remove any remaining microglia) after which the cells were spun down (5 minutes at 1000 RPM). Cells were resuspended in 5 ml culture medium, gently triturated through a 21-gauge needle, counted, and plated at a density of 50,000 cells in a 20 µl droplet of SATO medium [DMEM with 1% pen/strep. 1% ITS supplement (Sigma-Aldrich), 16 µg/ml putrescine (Sigma-Aldrich), 400 ng/ml L-thyroxine (Sigma-Aldrich), 400 ng/ml Tri-iodothyroxine (Sigma-Aldrich), 60 ng/ml progesterone (Sigma-Aldrich), 100 µg/ml BSA (fraction V) (Sigma-Aldrich)] per PDL coated coverslip in a 24 well plate, topped up to 0.5

ml SATO medium per well after 20 minutes at 37°C for cells to stick down. OPCs were grown for 2 days and the medium was not changed during this time.

Conditioned media experiments

Collection of conditioned media. Endothelial cells (HUVECs, BMECs and bEND.3 cells) were grown in normal culture medium until reaching confluence and forming tight junctions [~10 days in vitro (DIV) for BMECs, 5 DIV for bEND.3 cells]. At this point the media was changed for media of the target culture (SATO medium, microglia medium, or slice medium), and this was conditioned for 2-3 days. Media was then removed and stored at -20°C until required. Media was filtered with a Millex 0.22 μm syringe filter prior to use.

Experiments using conditioned media. Cells grown in conditioned media were prepared as normal. Conditioned media was added to OPCs after the step at which they were left for 20 minutes to stick down. Cells were left for 2 days in conditioned media before being fixed and analyzed. Slices grown in conditioned media were prepared as normal. After preparation, slices were grown in normal media for 1 day to settle into culture, before the media was changed for 0.8 ml of conditioned media. Media was changed for fresh conditioned media every 2-3 days, and slices were grown for 5 weeks before being fixed and analyzed.

HSP90α experiments. Recombinant HSP90α (Enzo Life Sciences; ADI-SPP-776-D) was added to media at 1 μg/ml, and HSP90α blocking antibody (Enzo Life Sciences; ADI-SPS-771-D) was added to media at 1.7 μg/ml, as successfully used previously (*75*).

Treatment of bEND.3 cells with siRNA

After splitting, bEND.3 cells were plated at half confluent density in a 24-well plate (day 0). After 1 DIV, the media was changed and cells were transfected with pre-mixed siRNA (5pmol per well; Ambion; *Atp11b*: sense: GGGUGAUAUUGUUCGUAUAtt; Non-targeting: sense:

UUACGUCGUCGCGUCGUUAtt) and lipofectamine RNAiMAX (3 µl per well; Life Technologies) diluted in Opti-MEM (Life Technologies). At 4 DIV, media was changed and cells were again transfected with pre-mixed siRNA and lipofectamine RNAiMAX. Cells were fixed and analyzed at 7 DIV. To determine the efficiency of the knockdown, protein was extracted from unfixed cells at 7 DIV.

Treatment of human endothelial cells with siRNA

HUVECs were plated at 10^5 cells per well in a 6-well plate (day 0). After 1 DIV, the media was changed and cells were transfected with pre-mixed siRNA (1 µl per well; Dharmacon ON-TARGETplus SMARTpool; *ATP11B*: sense: GAAGAGGUUACGGCAUA, GCUAAGAACUCUGUGUAUA, GGUACAAACUGCUUCAUAU, AAAUGGAGCUCCUGUUUAU; Non-targeting: sense: UGGUUUACAUGUCGACUAA, UGGUUUACAGUGGGUGUGA, UGGUUUACAUGUUUUCUGA, UGGUUUACAUGUUUUCCUA) and lipofectamine RNAiMAX (3µl per well; Life Technologies) diluted in Opti-MEM (Life Technologies). To determine the efficiency of the knockdown, protein was extracted from unfixed cells at 7 DIV.

Immunostaining

Fluorescent immunohistochemistry (IHC) on paraffin embedded rat tissue. Sections were deparaffinized by immersion in Xylene (2x 5 minutes; Fisher) and rehydrated by immersion in descending concentrations of ethanol (100%, 90%, 80%, 70%, 50%, 30%; 1 minute each) before being immersed in PBS. Antigen retrieval was carried out by boiling sections for 15 minutes in a microwave in citrate buffer (Vector). Sections were then cooled for 20 minutes in running tap water. Sections were blocked for at least 1.5 hours at room temperature in blocking solution [10% heat inactivated horse serum (HIHS), 0.3% triton (Fisher) in PBS]. Primary antibodies, diluted in blocking solution, were added and the sections were incubated at 4°C overnight in a humid chamber. The sections were washed in PBS (3x 5 minutes), then secondary antibodies, diluted in blocking solution, were added for 1.5 hours at room temperature (RT). Sections were washed in PBS (3x 5 minutes), Hoechst (VWR) was then added (1 minute), and then sections were washed again in PBS (5 minutes). Sections were mounted with Fluoromount (Southern Biotech).

Fluorescent IHC on fixed, frozen rat tissue. IHC was carried out as above for paraffin fixed rat tissue, but without deparaffinization or antigen retrieval steps.

Fluorescent IHC on paraffin embedded human tissue. IHC was carried out as above for paraffin fixed rat tissue, with a signal enhancing step [30-minute incubation with iFX signal enhancer (Molecular Probes), 5 minute PBS wash] immediately prior to blocking and an autofluorescence quenching step [5 minute incubation with Sudan black (0.01% in 70% ethanol; Sigma-Aldrich), 5 minute wash in 70% ethanol, 5 minute wash in PBS] immediately prior to mounting.

Colorimetric IHC on paraffin embedded human tissue. Sections were deparaffinized and antigen retrieval carried out as described above for paraffin embedded rat tissue. Endogenous enzyme activity was blocked with Vector Bloxall (10 minutes) then sections were washed with PBS (5 minutes). Sections were blocked with 2.5% normal horse serum (NHS; from Vector ImmPress kit; 20 minutes) then washed with PBS (5 minutes). First primary antibody, diluted in antibody diluent (Spring Bioscience) was incubated overnight in a humid chamber at 4^{o}C. Sections were washed in PBS (5 minutes) and Vector ImmPress secondary was added for 1 hour at RT. Antibodies were visualized with Vector horseradish peroxidase (HRP) NovaRED for 10 minutes before washing in PBS (5 minutes) to stop the reaction. Sections were then blocked with 2.5% NHS (20 minutes) before the second primary antibody, diluted in antibody diluent, was added (overnight in humid chamber, 4^{o}C). Sections were washed in PBS (5 minutes) and Vector ImmPress secondary was added for 1 hour at RT. Sections were visualized with Vector alkaline phosphatase (AP) Blue for 30 minutes, before washing in PBS (5 minutes) to stop the reaction. Sections were then rinsed in distilled water before mounting with Fluoromount.

Fluorescent IHC on ex vivo brain slices. Slices were fixed in 4% PFA for 1 hour before being rinsed in PBS. The outer plastic ring of the cell culture insert was then removed and the slices were further washed in PBS (3x 10 minutes). Slices were incubated with blocking solution [3% HIHS, 2% bovine serum albumin (BSA; Sigma-Aldrich), 0.5% triton in PBS] for 2 hours at RT on a rocker. Primary antibodies,

diluted in blocking solution, were added either overnight at RT on a rocker, or for 2 nights at 4°C on a rocker (conditioned media experiments only). Slices were washed in blocking solution (10 minutes, then 3x 1 hour) before the secondary antibodies were added overnight at RT on a rocker. Slices were washed with PBS (10 minutes, then 3x 1 hour) then Hoechst was added (1 minute). Slices were rinsed in PBS and mounted with Fluoromount.

Immunocytochemistry (ICC). Cells were fixed in 4% PFA (10 minutes) then washed with PBS (3x 5 minutes). Blocking solution (10% HIHS, 0.1% triton in PBS) was added for 1-1.5 hour at RT on a rocker. Cells were then incubated with primary antibodies, diluted in blocking solution, for 1-1.5 hour at RT on a rocker. Cells were washed with PBS (3x 2 minutes) then incubated with secondary antibodies, diluted in blocking solution, for 1 hour at RT on a rocker. Cells were washed with PBS (3x 2 minutes), Hoechst added (1 minute) and washed again with PBS (rinse then 2 minutes) before being mounted with Fluoromount.

Primary antibodies used. CD34 (1:80; Santa Cruz; sc-7045), CD68 (1:100; Abcam; ab5344; ICC only), CD68 (1:100; Dako; M0814), claudin-5 (1:100; Zymed; 34-1600), claudin-5 (1:100; Abcam; ab53765), fluorescein (1:100; Abcam; ab6655), GFAP (1:500; Dako; Z0334), Iba1 (1:500; Wako; 019-19741), Ki67 (1:200; Abcam; ab9160; ICC only), Ki67 (1:200; Abcam; ab16667; ICC only), MBP (1:300; AbD Serotec; MCA4095), NG2 (1:200; Merck Millipore; MAB5384; ICC only), NG2 (1:200; Merck Millipore; AB5320; ICC only), Nogo-A (1:100; R&D Systems; MAB3098), Olig2 (1:100; Merck Millipore; ab9610), Olig2 (1:100; Atlas Antibodies; HPA003254), PCNA (1:200; Dako; M0879), PDGFR-β (1:100; Abcam; ab32570), ZO-1 (1:100; Life Technologies; 33-9100; ICC only).

Analysis of proteins

Extraction of protein from tissue. Areas of basal ganglia from fresh, frozen sections of brain tissue, cut using a cryostat onto glass slides, were scraped off with a razor into a solution of 400 µl of radioimmunoprecipitation assay (RIPA) buffer (Pierce) with 1% protease inhibitor (PI; Calbiochem),

aiming for a total of approximately 10 mg (10 µl by volume size) of tissue. This was homogenized by hand on ice with a plastic pestle before being sonicated (3x 10 seconds sonication followed by 10 seconds on ice). This was spun down in a microfuge (20 minutes, 13,000 RPM, 4°C) and the supernatant transferred to fresh tubes in 50 µl aliquots.

Extraction of protein from cells. Culture media was removed from wells and approximately 50 µl of RIPA buffer with 1% PI was added to each well (of a 24 well plate). Cells were scraped with a bent pipette tip and the resultant liquid transferred to a tube. This was spun down in a microfuge (10 minutes, 13,000 RPM, 4°C) and the supernatant collected.

Quantification of total protein. Protein levels were quantified using a bicinchoninic acid assay (BCA assay), using solutions from a Pierce BCA protein assay kit. BCA working solution was prepared as specified, and 200 µl added to each well of a flat-bottomed 96-well plate. 10 µl of sample was added to each relevant well, and 9 wells were used for a BSA standard curve (0 µg/ml to 2000 µg/ml in RIPA). The plate was incubated at 37°C for 30 minutes and then allowed to cool to RT. The absorbance of each well at 562 nm was measured using an Omega Plate Reader. Protein concentration of each sample was then calculated by comparison to the standard curve.

Western blotting. Protein lysates were diluted in RIPA and 4x Laemmli buffer [8% sodium dodecyl sulphate (SDS), 40% glycerol, 20% β-mercaptoethanol, 0.4% bromophenol blue, 0.25M Trizma hydrochloride; all from Sigma-Aldrich] to a concentration of 5 µg of protein in 20 µl (20 µg of protein in 30 µl for ATP11B) in 1x Laemmli buffer. Samples were then boiled at 95°C for 5 minutes and loaded into Pierce ready-cast 4-20% Tris-HEPES gels, in a gel tank filled with HEPES running buffer (Pierce) or Bio-Rad 4-15% Mini-PROTEAN TGX Precast Protein Gels, (Bio-Rad) in gel tank filled with 10X TGS running buffer (Bio-Rad). Samples were run, along with a protein ladder (Bio-Rad) for 1.5 hours at 100 Volts. The gel was then removed and placed into a transfer cassette with a polyvinylidene fluoride (PVDF) membrane [Merck Millipore; activated in methanol (Fisher)]. Gels were transferred in transfer buffer [20 mM Trizma base (Sigma-Aldrich), 150 mM glycine (Sigma-Aldrich), or 20% methanol in

water or 5% NuPage transfer buffer, 10% methanol in distilled water] for 2 hours at 400 mAmps or 1.5 hours at 160mAmps on ice. The membrane was removed from the cassette, washed in TBST [tris buffered saline (TBS; 20 mM Trizma base, 150 mM sodium chloride (Sigma-Aldrich), 2.7 mM potassium chloride (Fisher) in water) + 0.1% tween; PBST (PBS + 0.05% tween) for ATP11B] and blocked with 4% BSA in TBST (5% milk in PBST for ATP11B) for 1 hour at RT on a rocker. The membrane was then incubated with primary antibodies diluted in block overnight at 4°C on a rocker. The membrane was washed with TBST (3x 10 minutes; PBST for ATP11B) then incubated with secondary antibodies in block (half as diluted for ATP11B) for 1 hour (2 hours for ATP11B) at RT on a rocker. The membrane was then washed with TBST (PBST for ATP11B) and ECL substrate (Thermo Fisher; femto kit for ATP11B) was put on the membrane for 5 minutes. The excess was dabbed off and the membrane was either exposed to a film that was then developed, or imaged using a LiCor scanner.

Primary antibodies for western blot. ATP11B (1:250; Abcam; ab82640), claudin-5 (1:1,000; Zymed; 34-1600), eNOS (1:1,000; Abcam; ab5589), GAPDH (1:1,000; Merck Millipore; MAB374), HSP90α (1:1,000; Abcam; ab59459), HSP90α (1:1,000; Enzo Life Sciences; ADI-SPS-771-D).

ELISA for HSP90a

HSP90AA1 ELISA Kit (Aviva Systems Biology) was used according to the manufacturers' instructions. Briefly, 100 µl/well standards, samples and blanks were added to the microplate and incubated at 37°C for 2 hours. The liquid was discarded and 100 µl/well HSPAA1 detector antibody added for incubation at 37°C for 1 hour. After washing, 100 µl/well Avidin-HRP Conjugate was added and incubated at 37°C for 1 hour. After washing, 90 µl/well TMB substrate was added, followed by 50 µl/well stop solution after 30 minutes. O.D. absorbance was read at 450 nm with a standard microplate reader.

Antibody array

The antibody array was using a kit from Full Moon BioSystems (SET100) and was carried out as specified in their protocol.

Molecular biology

Extraction of deoxyribonucleic acid (DNA). Tail clips or ear punches from SHRSP and WKY rats were incubated in lysis buffer (1M Trizma hydrochloride), 0.5 M EDTA (Sigma-Aldrich), 5M sodium chloride, 10% SDS in water) with 10% proteinase K (Promega) overnight at 55°C. The samples were then incubated at 95°C for 10 minutes, followed by an incubation at 0°C for 15 minutes. The samples were centrifuged for 10 minutes and the supernatant collected. This supernatant was diluted 1:10 for polymerase chain reaction.

Extraction of ribonucleic acid (RNA). RNA was extracted from BMECs using the Qiagen RNeasy mini kit exactly as specified in the kit's protocol. RNA samples were kept in water at -80°C until synthesis of complement DNA (cDNA).

Synthesis of complement DNA (cDNA). All reagents came as part of SuperScript First-Strand Synthesis System for RT-PCR. 3-8 µl of RNA was mixed with 1 µl deoxynucleotides (dNTPs) and 1 µl hexamer primers (filled up with water to a total volume of 10 µl) and incubated for 5 minutes at 65°C. After cooling down for 1 minute on ice, an additional reaction mix was added (2 µl RT buffer, 4 µl $MgCl_2$, 2 µl DTT, 1 µl RNase OUT) and incubated for 2 minutes at RT. Then, 1 µl Superscript II was added and the samples were incubated for 10 minutes at. Subsequently, samples were incubated at 42°C (50 min) and 70°C (15 min). cDNA synthesis was completed by adding 1 µl RNAse H and incubating at 37°C for 20 minutes.

Polymerase chain reaction (PCR). PCR was carried out using Promega GoTaq Hot Start Polymerase, which included all the reagents required. To the master mix (10 µl 5X PCR buffer, 4 µl 25mM $MgCl_2$, 1 µl dNTPs, 5µl each of forward and reverse primers (1:10), 0.25 µl GoTaq in 22.75 µl water per reaction) 2 µl of DNA sample was added. After activation of GoTaq polymerase, 30 cycles of amplification were carried out, followed by denaturation by a 2 minute incubation at 94 °C. A touch-down protocol was used for the annealing phase (60-48 °C). For the elongation stage, samples were held at 72 °C for 5 minutes. After the PCR was complete, samples were mixed with dye and visualized on a 1.3% agarose gel to

confirm that the reaction worked. PCR products for sequencing were purified using QIAquick PCR purification kit following the provided protocol.

Sequencing of DNA/complement DNA (cDNA). Primers were designed, using NCBI primer blast, 300-500 bases either side of the predicted mutation site (*Atp11b*: forward: AAAGGCTACCTACTTGGTTGGG, reverse: CAATACTCTCTTCCGCCCACAG; *Atp11b* cDNA: forward: CCGCAGAAGGAAATGACCCT, reverse: CTCCTGGCAAGCTGTCTCAA) and the relevant region of (c)DNA was amplified using these primers by PCR. These products were 600-1,000 bases long as any sequencing reads in the first 100 bases or after 800 bases can sometimes be unreliable. These PCR products were sent off, along with forward and reverse primers around the predicted mutation site, to Source Bioscience for sequencing, according to their specifications (16 pmol in 5 µl of primers per reaction, 50 ng in 5 µl of each sample per reaction). Sequences were aligned using BioEdit Sequence Alignment Editor (Ibis Biosciences).

Assay of nitric oxide synthase (NOS) activity

NOS activity was measured using an assay kit from Merck Millipore which reduced all nitrates in conditioned media to nitrites, and quantified this based on a color change when Griess reagents were added.

Imaging and analysis

Imaging. Fluorescent images were captured using Leica SPE and Leica SP8 confocal microscope systems. Colorimetric images were captured using an AxioScan Slide Scanner.

Image analysis. All immunostained images were quantified using the FIJI build of ImageJ software (open source). Cells were counted using the Cell Counter plugin. ICC and drug study IHC images were blinded before quantification. Other IHC images were not blinded prior to quantification, however a random selection was quantified again after blinding to confirm the reliability of the quantification. On brain sections, at least five fields of view from the deep white matter and basal ganglia were analyzed per

subject. For *in vitro* experiments at least three fields of view from each of a minimum of two wells were analyzed per biological repeat.

Quantification of western blots. Western blots were analyzed using the Western Blot Quantification tool in FIJI, or Image Studio Lite (LI-COR Biosciences), to give the relative intensity of different bands. These were then normalized to the sample loading control.

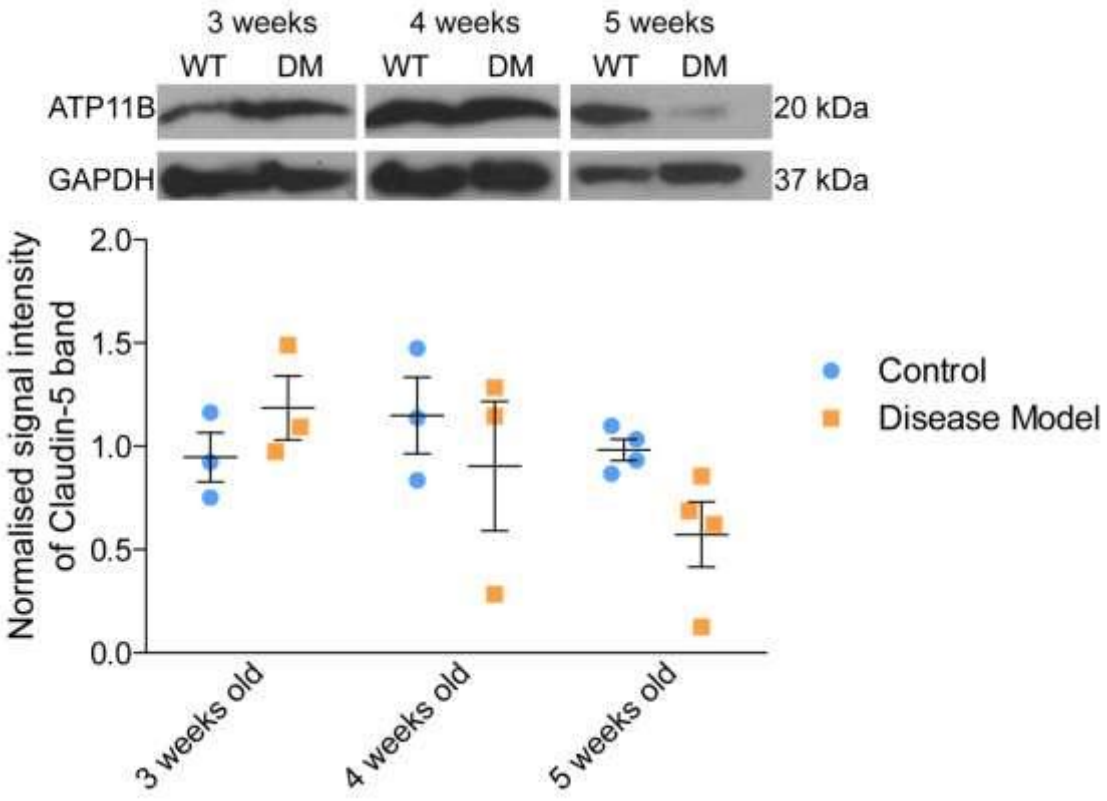

Fig. S1. Lower claudin-5 protein in brains of DM rats. Representative western blots of claudin-5 in the brains of DM rats compared to controls from 5 weeks of age, with GAPDH shown as loading control. Graph shows densitometry ratios of Claudin-5 to GAPDH for western blots of brain samples from each of three animals per time-point. (Mean +/- SEM; 3wk, 4wk: n=3 animals; 5wk: n=4 animals).

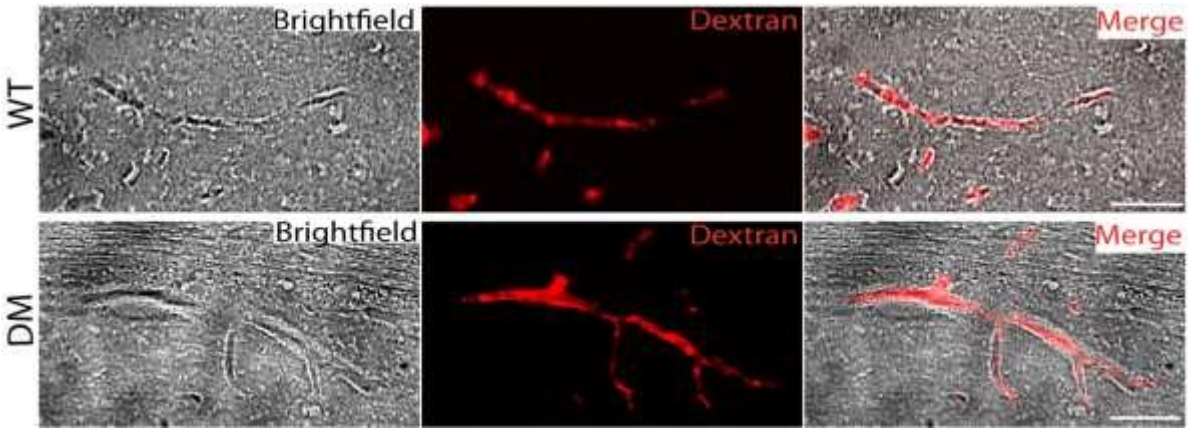

Fig. S2. **No leakage of a large dextran tracer indicates normal vascular integrity in 5-week-old DM rats.** There is no leak of 65-85 kD dextran outside the blood vessel walls in 5-week-old DM rats in spite of fewer claudin-5 positive tight junctions. Dextran tracer (red) and bright-field images. Scale bar = 50 μm.

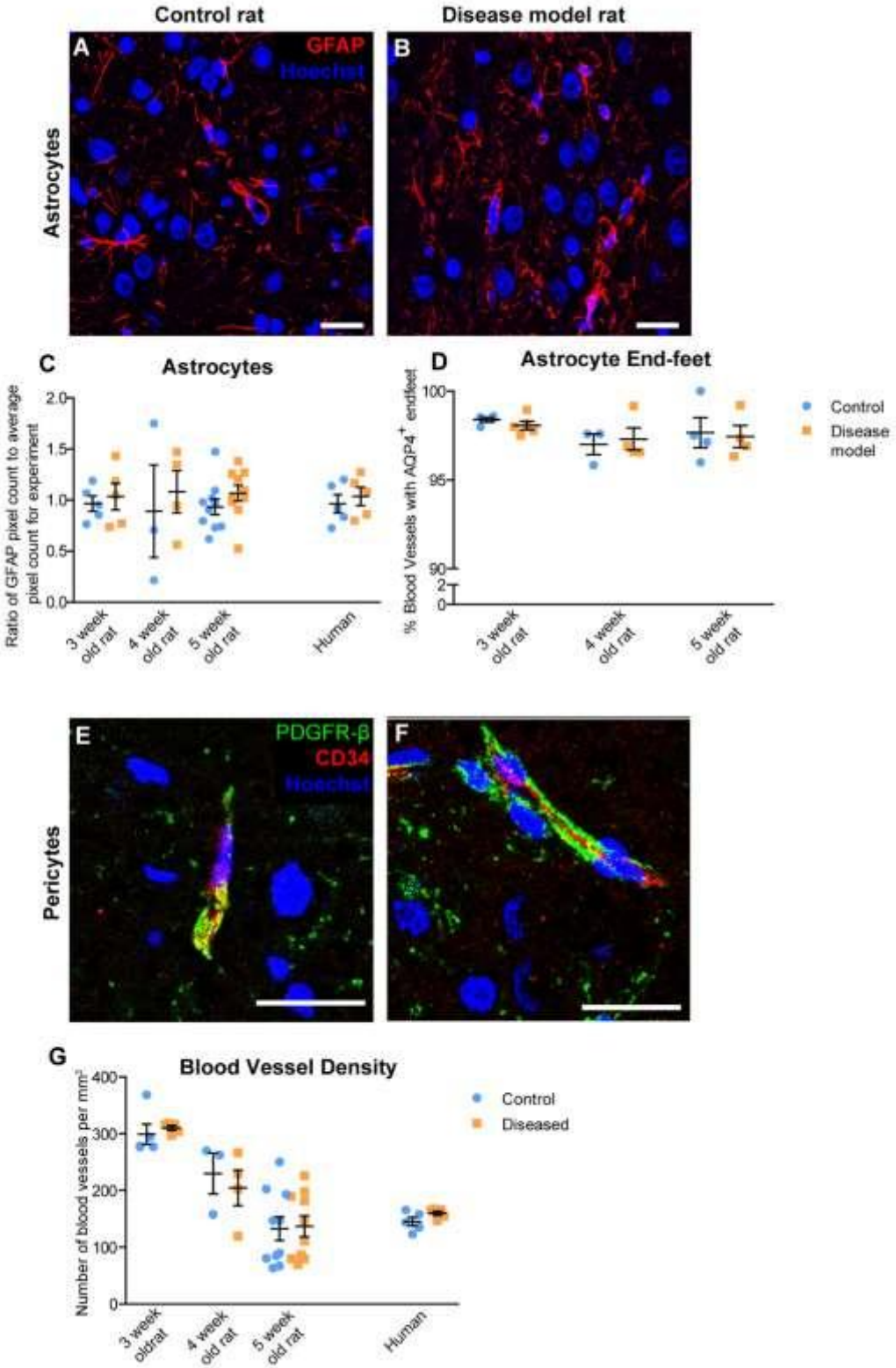
Control rat
Disease model rat
A
B
GFAP
Hoechst
Astrocytes
C
Astrocytes
Ratio of GFAP pixel count to average pixel count for experiment
2.0
1.5
1.0
0.5
0.0
3 week old rat
4 week old rat
5 week old rat
Human
D
Astrocyte End-feet
% Blood Vessels with AQP4+ endfeet
100
95
90
2
0
3 week old rat
4 week old rat
5 week old rat
Control
Disease model
E
F
PDGFR-β
CD34
Hoechst
Pericytes
G
Blood Vessel Density
Number of blood vessels per mm2
400
300
200
100
0
3 week oldrat
4 week old rat
5 week old rat
Human
Control
Diseased

Fig. S3. No difference in astrocytes or pericytes. A-B: Immunofluorescent images showing GFAP (astrocytes; red), and Hoechst (blue), in the deep white matter of rat brains. **C**: Pixel counts of GFAP staining in rats and humans were normalized to the average level of staining for each experiment to account for variations between different batches of immunostaining. (Mean ± SEM; 3wk: n=5 animals; 4wk: n≥3 animals; 5wk: n=10 animals; human: n=5). **D**: Percentage of blood vessels with aquaporin 4 (AQP4) positive astrocyte end-feet around them. (DM rats (orange), controls (blue), Mean ± SEM; 3wk, 4wk: n≥3 animals; 5wk: n=4 animals). **E-F**: Immunofluorescent images showing normal morphology of PDGFR-β^+ pericytes (green), in brains from 5-week-old control (**E**) and DM (**F**) rats, with endothelial cells ($CD34^+$; red) and Hoechst (blue). **G**: Quantification of blood vessel number per mm^2 for control and DM rats, and control and diseased human brains (based on images in Fig. 1). Scale bar = 25 μm.

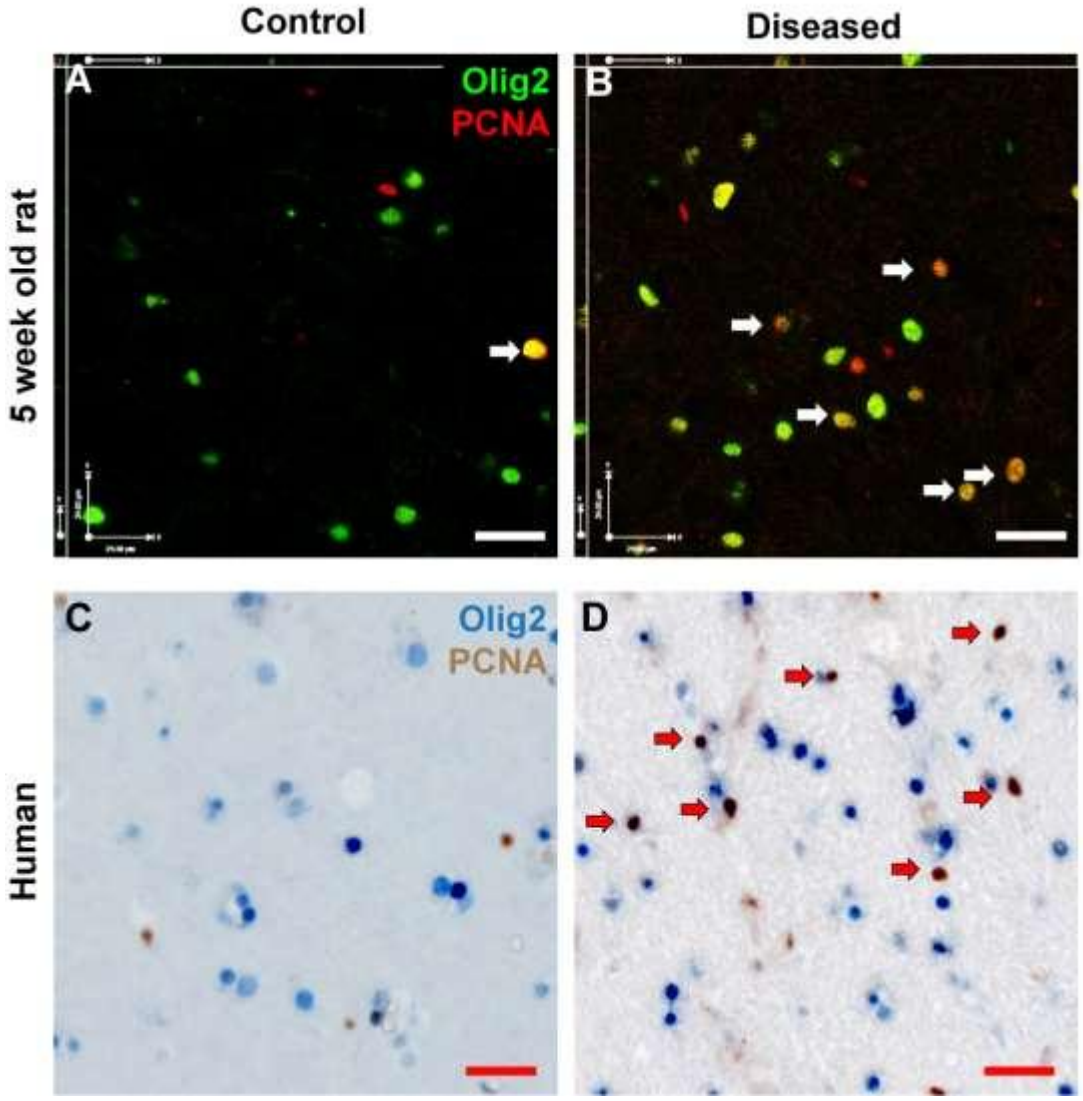

Fig. S4. Increased number of OPCs due to increased proliferation in DM rats and diseased human brains. **A**-**B**: Immunofluorescent images showing Olig2 (all oligodendroglia; green), and proliferating cell nuclear antigen (PCNA; proliferating nuclei; red), in the deep white matter of brains from 5-week-old control (**A**) and DM rats (**B**). **C**-**D**: Images showing colorimetric immunostaining of Olig2 (blue) and PCNA (brown) in the deep white matter of control (**C**) and diseased (**D**) human brains. Arrows indicate proliferating OPCs ($Olig2^+$ $PCNA^+$). Quantification in Fig. 1P. Scale bar = 25 μm.

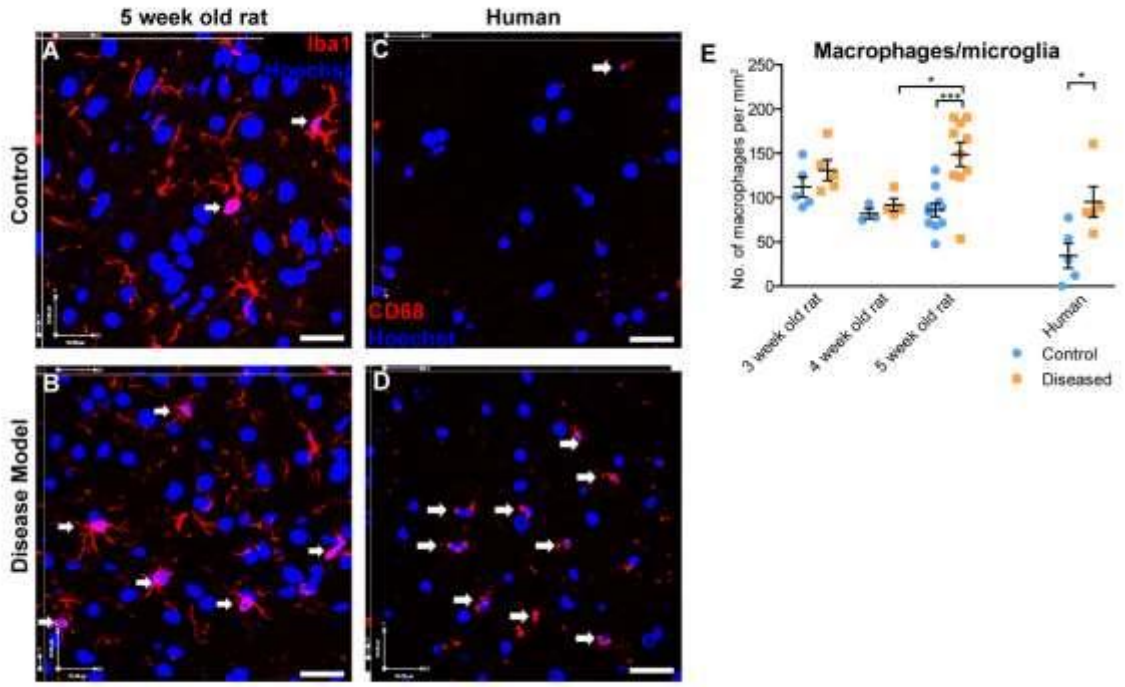

Fig. S5. Brains of young, pre-hypertensive DM rats and pre-symptomatic humans show increased numbers of microglia/macrophages. Immunofluorescent images, taken from sections of deep white matter from the brains of control (**A**) and DM (**B**) rats and control (**C**) and diseased (**D**) human brains, showing staining for Iba1 (**A**-**B**), a marker of all macrophages and microglia, or CD68 (**C**-**D**), a marker of activated macrophages and microglia (red), and Hoechst, a nuclear marker (blue). Quantification of the number of macrophages/microglia per mm^2 (**E**) (Mean ± SEM; ***: $P<0.001$, *: $P<0.05$, two-way ANOVA with Tukey's post-hoc tests; 3wk: n=5 animals; 4wk: n≥3 animals; 5wk: n=10 animals; human: n=5). Scale bar = 25 μm.

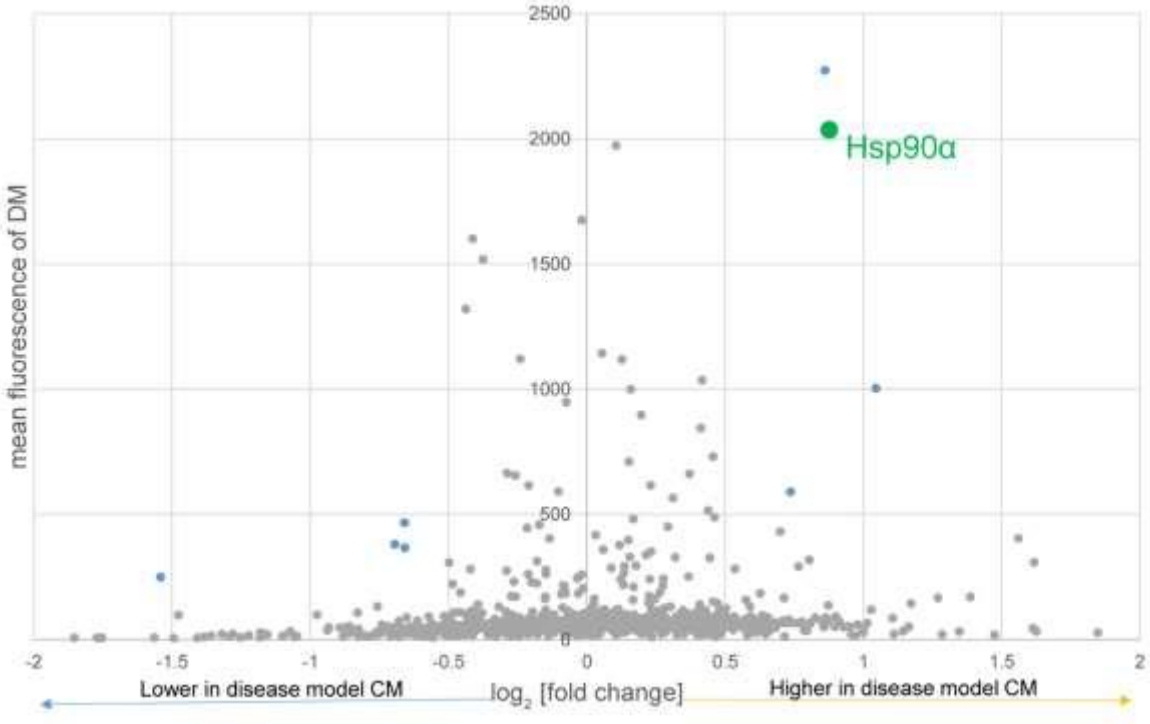

Fig. S6. More HSP90α is secreted by BMECs isolated from DM rats. Graph showing the results from the Full Moon Signalling Explorer antibody array. Each point represents a different protein detected by the array. The y-axis shows the mean fluorescence of the spots for that protein on the array of the DM conditioned media (CM). The x-axis shows the $\log_2$ of the fold change between the DM CM and control CM (brightness of spot in DM CM divided by brightness of spot in control CM). Points further to the right represent proteins which are higher in DM CM, whereas those on the left represent proteins which are lower in DM CM compared to controls. Spots with a mean fluorescence below 400 are unreliable (too close to the negative control) and those with $\log_2$ [fold change] less than 0.5 do not show large differences between DM and control CM. These proteins are represented in grey, whereas potential proteins of interest are shown in blue and green. HSP90α, indicated in green, was chosen as the first candidate to investigate.

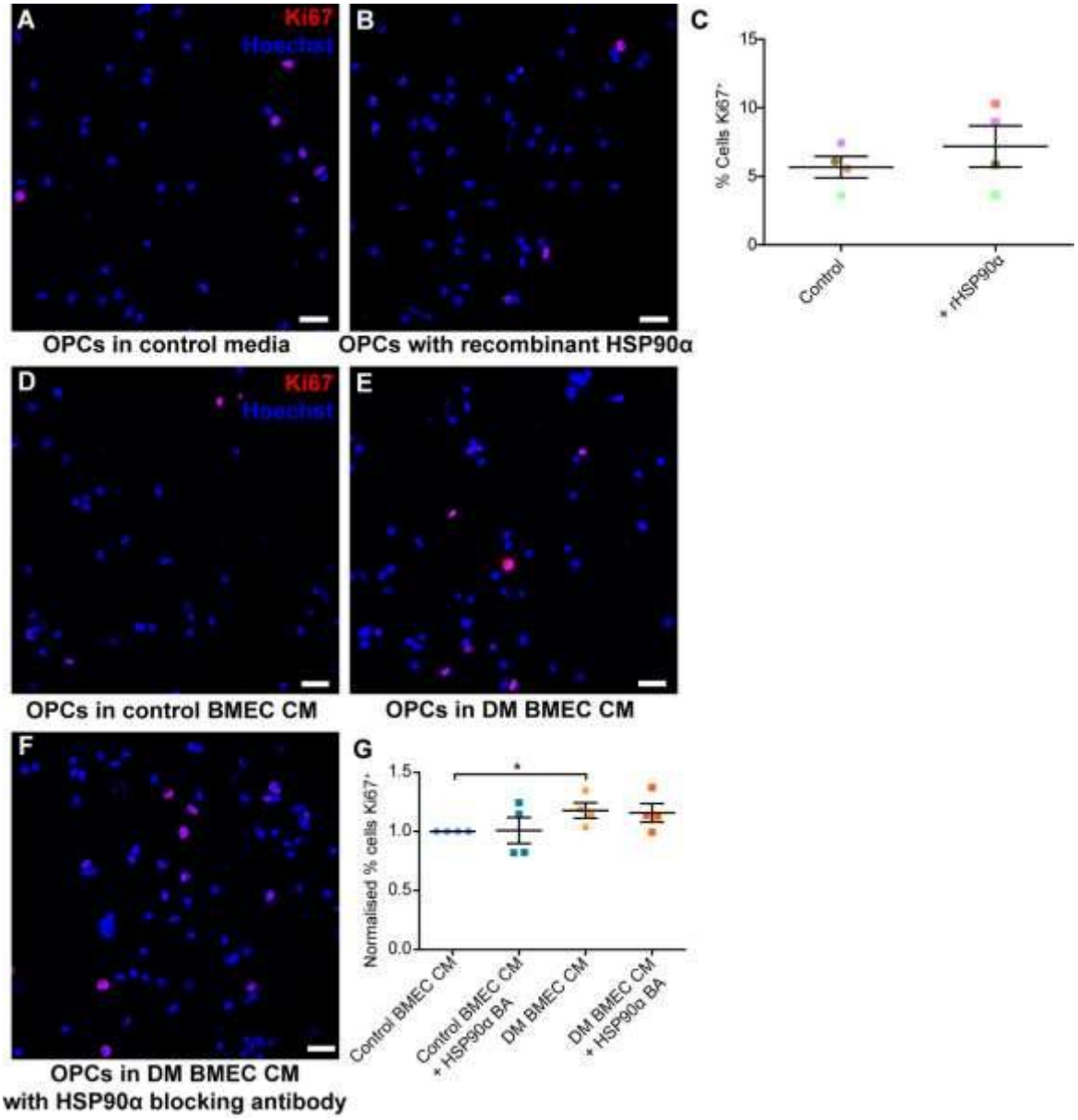
A
Ki67
Hoechst
B
C
15
10
5
0
% Cells Ki67+
Control
+ rHSP90α
OPCs in control media
OPCs with recombinant HSP90α
D
Ki67
Hoechst
E
OPCs in control BMEC CM
OPCs in DM BMEC CM
F
G
1.5
1.0
0.5
0.0
Normalised % cells Ki67+
*
Control BMEC CM
Control BMEC CM + HSP90α BA
DM BMEC CM
DM BMEC CM + HSP90α BA
OPCs in DM BMEC CM with HSP90α blocking antibody

Fig. S7. Addition of rHSP90α or use of blocking antibodies to HSP90α has no effect on OPC proliferation. A-B: Immunofluorescent images of the number of cells expressing Ki67 (proliferating nuclei; red), and Hoechst (blue), in cultures of OPCs grown in control conditions (**A**) and with rHSP90α (**B**) (n=4 separate experiments with cells from different litters. Quantified in **C** (Each color represents a different paired repeat)). **D-F**: Immunofluorescent images showing Ki67 (proliferating nuclei; red), and Hoechst (blue) in cultures of OPCs grown in control BMEC CM (**D**), DM BMEC CM (**E**), and DM BMEC CM with HSP90α blocking antibody (BA) added (**F**). **G**: Quantification of the percentage of proliferating $Ki67^+$ cells cultured in DM CM (orange) compared to control CM (blue), with and without HSP90α BA (squares). Data normalized to control CM such that 1 = an average of 18% $Ki67^+$. (Mean ± SEM; $p<0.05$, 1-way ANOVA with Bonferroni post-hoc tests; n=4 separate experiments with cells from different litters). Scale bar = 25 μm.

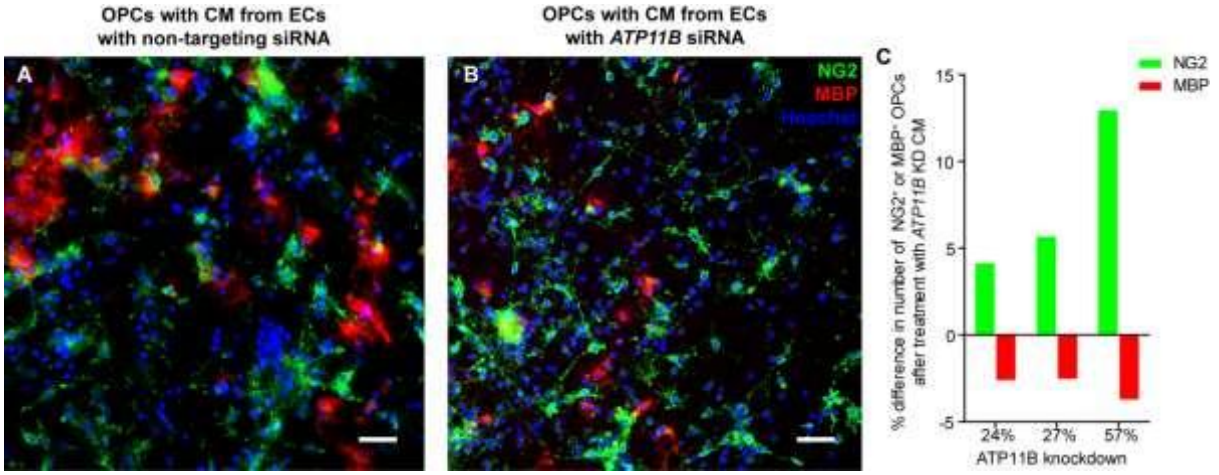

Fig. S8. Conditioned medium from human ECs treated with *ATP11B*-siRNA reduces OPC maturation. (**A-B**) Immunofluorescence of rat OPC cultures after treatment with CM from ECs treated with non-targeting siRNA (A) or siRNA knocking down *ATP11B* expression (B) showing $NG2^+$ cells (green) and MBP^+ cells (red). (**C**) Quantification of each treatment, separated by the degree of knock down of ATP11B (at protein level). Scale bar = 50 μm.

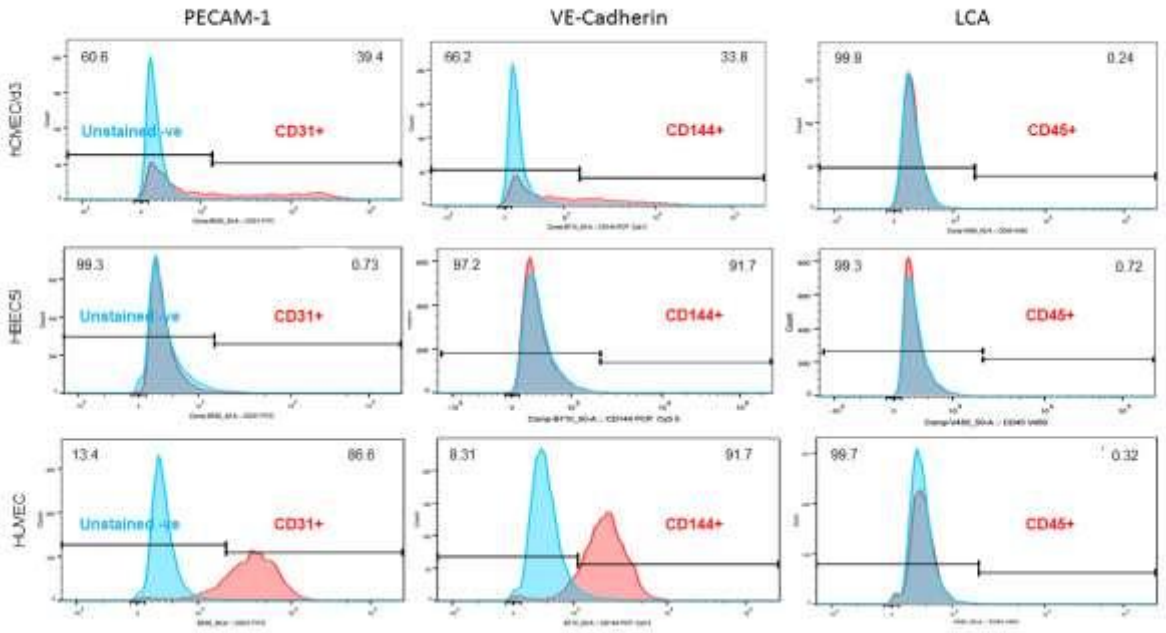

Fig. S9. Human cerebral endothelial cells from the HBEC5i and hCMEC/d3 lines do not express endothelial markers. Flow data of cultures of the cell line HBEC5i and hCMEC/d3 compared to HUVECs, with the endothelial markers CD31 (PECAM-1), CD144 (VE-Cadherin) and a non-endothelial marker CD45 (LCA).

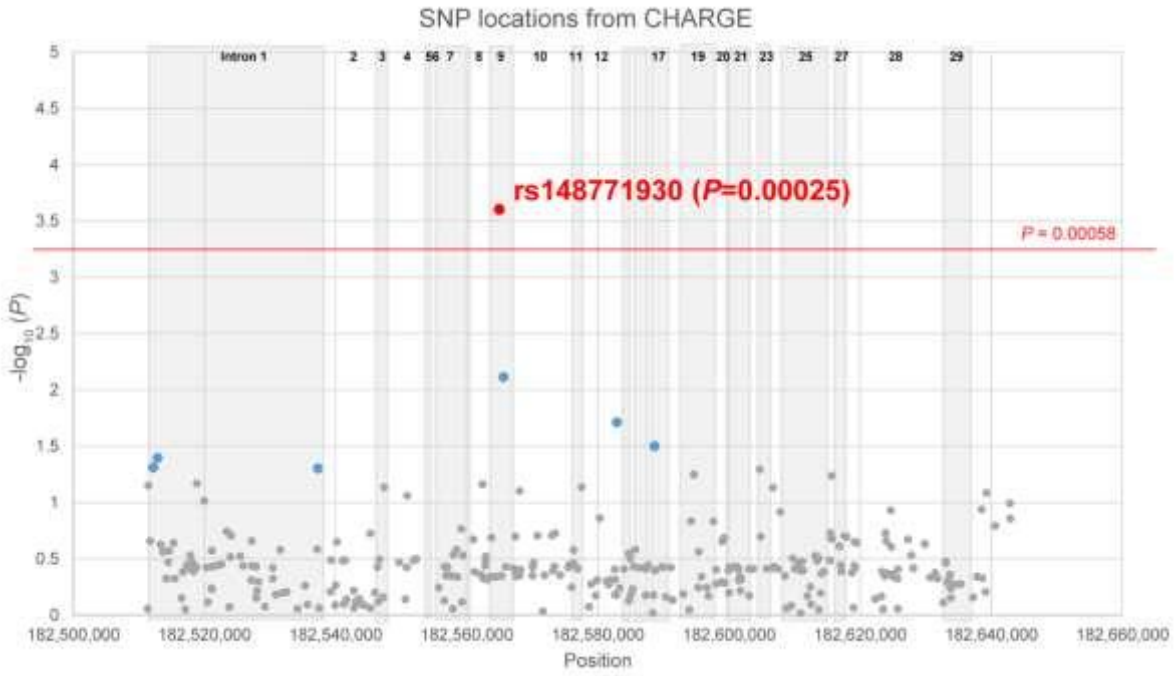

Fig. S10. SNPs within *ATP11B* are associated with WMH in the Cohorts for Heart and Aging Research in Genomic Epidemiology (CHARGE). Chart showing the location of SNPs investigated within *ATP11B*, with different introns indicated by alternating light and dark bands. The y-axis shows the $-\log_{10}(P)$ of the association of that SNP with WMH burden on magnetic resonance imaging (MRI), a marker of SVD. Data is from the CHARGE consortium and includes 17,936 individuals of European descent from 29 population-based cohorts (*40*). SNPs in grey are those with $P>0.05$, while those in blue and red are those with $P<0.05$. After correcting for multiple testing, using spectral decomposition to determine the number of independent SNPs tested using the 1000 Genomes reference as a measure of linkage disequilibrium (*41*) (modified significance value of $P<0.00058$), we found one SNP which was associated with WMH burden: rs148771930, indicated in red.

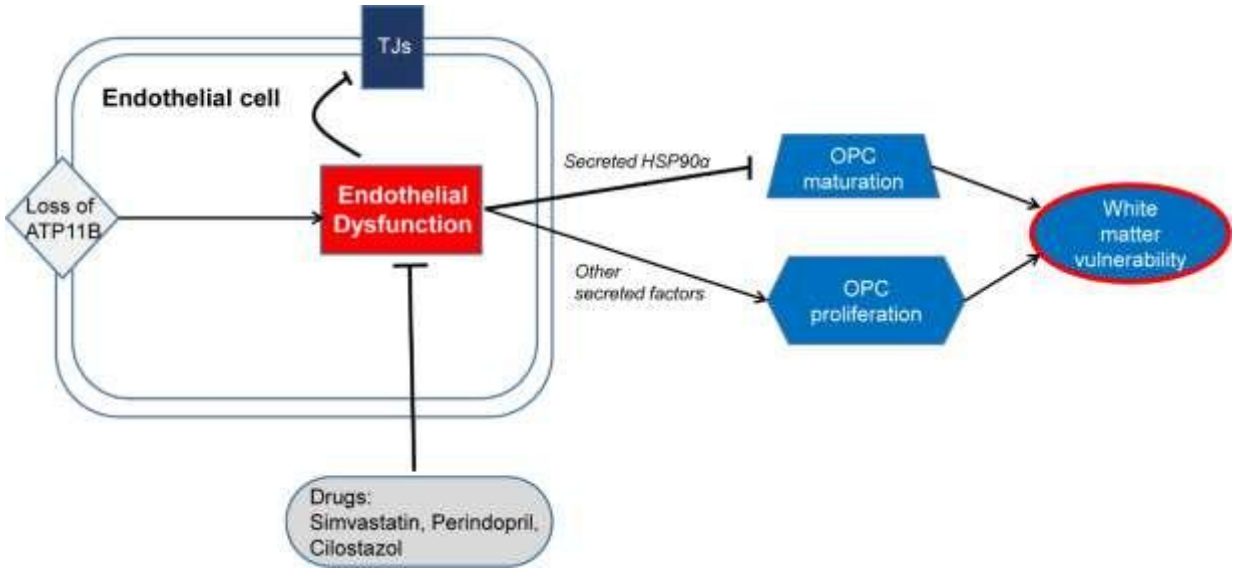

Fig. S11. Summary of findings, illustrating the central role of endothelial dysfunction in small vessel disease (SVD) pathology. Endothelial dysfunction manifests as reduced production of nitric oxide, endothelial cell (EC) proliferation, reduced tight junctions (TJs) and a weakened blood brain barrier (BBB). This BBB leakage may contribute to later progressive perivascular and white matter injury. Dysfunctional ECs secrete HSP90α, which inhibits oligodendrocyte precursor cell (OPC) maturation, increasing vulnerability to white matter lesions. Other as yet unidentified endothelial secreted factors stimulate OPC proliferation. Drugs, such as simvastatin, perindopril and cilostazol, can improve this endothelial dysfunction, restoring normal OPC maturation, OPC proliferation, and TJs. We show a genetic upstream cause of this endothelial dysfunction, a loss of ATP11B, however endothelial dysfunction may also occur through other genetic causes and/or environmental influences (smoking, hypertension, diabetes mellitus).

Table S1. Summary of human SVD and control post mortem data and pathological characteristics.

Controls						
Patient Number	**Gender**	**Age**	**Death Certificate**	**PM interval (hours)**	**Block**	**Neuropathology report**
SD015/08	M	53	Suspension by a ligature	42	2I	No significant abnormality.
SD021/08	M	44	Suspension by a ligature	83	2E	No significant abnormality.
SD034/08	M	70	Pulmonary embolism, Deep vein thrombosis, Hypertension, Previous pulmonary embolism	50	2F	No significant abnormality.
SD014/09	M	26	Methadone and diazepam toxicity	44	2F	The white matter appears unremarkable.
SD010/10	M	39	Sudden Adult Death	81	2K	White matter throughout appears unremarkable.
SVD						
Patient Number	**Gender**	**Age**	**Death Certificate**	**PM interval (hours)**	**Block**	**Neuropathology report**
SD019/08	M	58	Myocardial infarction, Small previous infarctions, Coronary arteriosclerosis, General arteriosclerosis, Heart disease	69	2H	Congestion within white matter. Some small vessels with thickened hyalinized walls.
SD020/08	M	51	Ischemic heart disease, Coronary arteriosclerosis, Heart disease	47	2E	White matter is congested. Some of the smaller vessels have thickened hyalinized walls with surrounding hemosiderin containing macrophages.
SD022/08	F	57	Pulmonary thromboembolism, Heart disease	95	2E	Small vessels with thickened hyalinised walls and surrounding hemosiderin containing macrophages
SD023/08	F	24	Suspension by a ligature	47	2H	Throughout the white matter there are scattered small vessels with thickened hyalinized walls and surrounding hemosiderin containing macrophages.
SD031/08	M	55	Acute myocardial ischemia, Coronary arteriosclerosis, Hypertension, Heart disease	31	2F	Throughout the white matter there are occasional vessels with thickened hyalinized walls.

Table S2. Summary of treatment groups in drug study. Table summarizing the treatment groups in the drug study including the control (Ctrl) and the 5 groups of disease model (DM) animals. The dosage of drug administered to each animal is shown, with the equivalent dose in humans [based on a conversion factor of 0.162 and a 60 kg human (*77*)] and the range of doses commonly given to humans. Also shown is the expected effect of each drug on reducing blood pressure and improving endothelial cell (EC) dysfunction.

Group	**Ctrl**	**DM 1**	**DM 2**	**DM 3**	**DM 4**	**DM 5**
Treatment	None	None	Simvastatin	Perindopril	Cilostazol	Hydrochlorothiazide + hydralazine
Type	-	-	Statin	ACEI	PDE3 inhibitor	Diuretic
Supplier	-	-	Sigma	Sigma	Sigma	Sigma
Daily dose	-	-	2 mg/kg/day	2 mg/kg/day	60 mg/kg/day	16 mg/kg/day of each
Human equivalent dose	-	-	19.44 mg/day	19.44 mg/day	583.2 mg/day	155.52 mg/day of each
Common human dose	-	-	5-80 mg/day	4-16 mg/day	100-400 mg/day	25-200 mg/day
Reduces blood pressure	-	-	-	✓	-	✓
Improves EC dysfunction	-	-	✓	✓	✓	-